EARLY MISSISSIPPIAN EVAPORITES OF COASTAL TROPICAL WETLANDS

DAVID MILLWARD*, SARAH J. DAVIES†, FIONA WILLIAMSON‡, RACHEL CURTIS†, TIMOTHY I. KEARSEY*, CARYS E. BENNETT†, JOHN E. A. MARSHALL‡ and MICHAEL A. E. BROWNE*

**British Geological Survey, The Lyell Centre, Edinburgh EH14 4AP, UK (E-mail: dmill@bgs.ac.uk)*

† School of Geography, Geology and the Environment, University of Leicester, Leicester LE1 7RH, UK

‡ Ocean and Earth Sciences, University of Southampton, National Oceanography Centre, European Way, Southampton SO14 3ZH, UK

Associate Editor – Jim Hendry

Short Title - *COASTAL WETLAND EVAPORITES*

http://dx.doi.org/10.1111/sed.12465

ABSTRACT

Extensive evaporites in Lower Mississippian successions from palaeoequatorial regions are commonly used as evidence for an arid to semi-arid palaeoclimate. However, in this study, detailed studies of evaporites and their context refute this interpretation. Detailed sedimentological and petrographical analysis of the Lower Mississippian of northern Britain, is combined with archived log data from more than 40 boreholes across southern Scotland, northern England and Northern Ireland, and published literature from Canada. Two key cores from the Tweed Basin and the northern margin of the Northumberland – Solway Basin contain 178 evaporite intervals and reveal twelve distinct forms of gypsum and anhydrite across seven facies that are associated with planar laminated siltstone and intercalated thin beds of ferroan dolostone. Nodular gypsum and anhydrite, typically in intervals less than 1 to 2 m thick, are integral components of the succession. Nodular evaporite occurs within about 1 m of a palaeosurface, but most evaporite deposits represent ephemeral brine pans to semi-permanent hypersaline lakes or salinas on a floodplain that was subjected periodically to storm surges introducing marine waters. Formation of evaporites under a strongly seasonal climate in a coastal wetland is supported by palaeosol types and geochemical proxies, and from palaeobotanical evidence published previously. Although 65% of modern equatorial areas experience a strongly seasonal climatic regime, salinas and sabkhas are a minor component today in comparison with the evidence from these Lower Mississippian successions. This implies that the earliest terrestrial environments were complex and dynamic providing a diverse range of habitats in which the early tetrapods became terrestrialized and represent a setting that is rarely preserved in the geological record.

Keywords Evaporite rock, monsoon, palaeoenvironment, tetrapod, Tournaisian.

INTRODUCTION

Two contrasting models for the early Mississippian climatic regime of southern Laurussia are presented in the literature: a humid climate (e.g. van der Zwan *et al*., 1985) with seasonality (e.g. Falcon-Lang, 1999) or an arid/semi-arid climate (e.g. Scott, 1986; Wright, 1982, 1990; Bateman & Scott, 1990; Andrews & Nabi, 1998). Understanding the climate and palaeoenvironments at this time is important because the terrestrialization of vertebrates occurred during the Tournaisian, following the end-Devonian mass extinction event (Kaiser *et al*., 2015). Climate and palaeoenvironment may be among the underlying factors that enabled this profound step in the evolution of life on Earth.

The early and mid Tournaisian humid climate proposed by van der Zwan *et al*. (1985) is supported by a number of UK-focussed studies (e.g. Hird & Tucker, 1988; Brofiscin Oolite, South Wales). In the Tournaisian of SE Scotland, Kearsey *et al*. (2016) linked the record of repeated river flood events (Bennett *et al*., 2016) with palaeosol data to conclude that the climate was tropical and markedly seasonal. These interpretations are consistent with the association of the reconstructed forest tree *Stamnostoma huttonense* with well drained palaeosols (Retallack & Dilcher, 1988) and the presence of growth rings in fossil wood (Falcon-Lang, 1999, 2004).

In contrast, other observations from the UK Tournaisian are cited as evidence for an arid or semi-arid climate, including the presence of calcretes in SE Scotland (Andrews & Nabi, 1998) and southern Britain (Wright, 1982, 1990) and the occurrence of evaporite rocks (Scott, 1986; Bateman & Scott, 1990). Young (1867) first recorded veins of fibrous gypsum cutting Tournaisian strata north of Glasgow, but the widespread occurrence of evaporite rock in this succession was revealed finally in a suite of boreholes drilled across the region by the British Geological Survey from the late 1960s onwards (e.g. Paterson & Hall, 1986).

For the first time, the current study describes a diverse suite of evaporite rocks from the lower Mississippian Ballagan Formation of northern Britain and interpret these within their host sedimentary succession (Bennett *et al*., 2016, 2017; Kearsey *et al*., 2016) and regional context,

discussing the implications for regional climate interpretations. This analysis provides an important insight into an unusual palaeonvironment with few modern analogues. The significance of this palaeoenvironment is increased in the light of new discoveries of vertebrate fossils with terrestrial capability in the Ballagan Formation and its correlative, the Horton Bluff Formation, in Nova Scotia (Clack, 2002; Smithson *et al*., 2012; Anderson *et al*., 2015; Clack *et al*., 2016).

GEOLOGICAL SETTING

In the Tournaisian, Nova Scotia and Scotland were located in equatorial latitudes on the southern margin of Laurussia (Domeier & Torsvik, 2014). Oblique dextral collision between Laurussia and Gondwana began in Famennian to Tournaisian times (Leeder, 1971, 1974; Leeder *et al*., 1989; Gawthorpe *et al*., 1989), and resulted in the fragmentation of part of the Laurussian margin to form a mosaic of linked sedimentary basins in the Midland Valley of Scotland and northern England (Coward, 1993). The early fill to these basins includes the Ballagan Formation (Figs 1 and 2), underlain by the Kinnesswood Formation and in the west overlain by the Clyde Sandstone Formation. The last two comprise similar facies. They consist of fluvial, cross-bedded sandstone in upward-fining cycles, interbedded with red and purple mudstone, multiple intervals with carbonate nodules and thin beds of concretionary limestone ('cornstones'; Read & Johnson, 1967; Eyles *et al*., 1949; Francis *et al*., 1970; Leeder, 1976; Leeder & Bridges, 1978; Young & Caldwell, 2011, 2012). The 'cornstones' are palaeosols containing extensive pedogenic carbonate and indicate a semi-arid or arid environment (Burgess, 1961; Leeder, 1976; Andrews *et al*., 1991; Wright *et al*., 1993). In the Scottish Borders, near Berwick upon Tweed, and along the northern margin of the Northumberland–Solway Basin, the Fell Sandstone Formation overlies the Ballagan Formation (Fig. 2).

Contrasting sharply with the units above and below, the Ballagan Formation consists dominantly of grey siltstone and thin beds of argillaceous ferroan dolostone (previously 'cementstone'), with varying proportions of sandstone, flood-deposited sandy siltstone, palaeosols and evaporite rock (Anderton, 1985; Scott, 1986; Andrews *et al*., 1991; Andrews & Nabi, 1994, 1998;

Bennett *et al*., 2016; Kearsey *et al*., 2016). The formation is best exposed in a 520 m thick, vertically dipping coastal section at Burnmouth (Fig. 1), bound by the Kinnesswood Formation at the base and Fell Sandstone Formation at the top (Fig. 2). In this section, and within the Norham West Mains Farm Borehole (see below), Bennett *et al*. (2016; table 1) identified ten facies and three facies associations within a coastal floodplain succession. The facies associations are fluvial, overbank, and saline – hypersaline lake. Evaporites occur mostly in the saline-hypersaline lake facies association, but are also present in the overbank facies association.

MATERIALS AND METHODS

This study combines data from the BGS borehole record collection with detailed studies of cores from three boreholes at the National Geological Repository, BGS Keyworth. The borehole logs archive contains *ca* 40 records that proved significant occurrences of the Ballagan Formation (Supplementary Data 1). Descriptive logs of 12 of these boreholes (Fig. 1), made in the past by BGS staff, provide consistent information on the spatial and temporal occurrence, context and general form of the evaporite deposits, though they do not contain sufficient sedimentological detail for facies analysis.

The Norham West Mains Farm Borehole located in the Tweed Basin about 10 km south-west of Berwick upon Tweed, fully cored 491 m of the Ballagan Formation (Fig. 1; Supplementary Data 1; Millward *et al*., 2013). Cores (102 mm diameter) were sliced lengthways and recorded by sedimentary logging at a scale of 1:12.5. Evaporite intervals were described from core, core photographs, hand specimens and polished thin sections. The Hoddom No. 2 Borehole was drilled near Ecclefechan on the northern margin of the Northumberland-Solway Basin in 1994 and the 48 mm diameter core was logged first by A. A. McMillan (BGS). For this study, the section beneath the base of the Fell Sandstone Formation, from 104.26 to 181.74 m was re-logged at the scale of 1:10. A visual inspection of the Glenrothes (Fife) Borehole core provided additional information. All depths quoted in this paper are below ground level.

Selected thin sections were examined using an Olympus BH52 petrographic microscope (Olympus, Tokyo, Japan) and the Hitachi S-3600N (Hitachi, Tokyo, Japan) and LEO1450 VPO (Zeiss, Oberkochen, Germany) scanning electron microscopes at the universities of Leicester and Southampton respectively. The elements present were determined using an Oxford INCA 350 EDX (Oxford Instruments, Abingdon, UK) energy dispersive X-ray spectrometer fitted to the former SEM. Dolomite descriptions follow the scheme of Sibley & Gregg (1987).

EVAPORITE OCCURRENCE AND DISTRIBUTION

Across the Midland Valley, evaporite rock occurrences are recorded as gypsum, along with sporadic records of siltstone pseudomorphs after halite (Figs 1 and 3). By contrast, gypsum and anhydrite are recorded from the upper and lower parts respectively of the Norham and Hoddom boreholes in the Tweed and Northumberland basins (Fig. 4). SEM analysis showed the presence of celestine, containing some barium, filling pore space and as tiny veins in dolostone associated with the evaporite rocks. In addition, Scott (1986) reported small amounts of barite from calcified nodules in dolostone beds at Burnmouth. No other evaporite species has been recorded.

These occurrences are small-scale, localized, and cannot be correlated between boreholes. Evaporite rock is absent from the succession in boreholes along northern and NE flanks of the Southern Uplands. Also, it is absent where the formation thins towards the northern margin of the Midland Valley, for example on the isles of Bute and Arran (Young & Caldwell, 2011, 2012).

The distribution of evaporite intervals is uneven through the formation (Figs 3 and 4). In the Deaconhill Borehole, for example, 12 intervals are present in the middle of the formation, whereas the 34 in the Blairmulloch Borehole are from the lower part. The 114 levels in the East Dron Borehole occur in all but the uppermost, sand-rich succession and basal Mains of Errol Member, though scattered pseudomorphs after gypsum are present in the latter (Browne, 1980). In the Norham core, the 50 occurrences are throughout the succession, with 24 concentrated in the lowest

80 m. In the Hoddom core, 128 intervals occur between depths of 131 m and the base of the borehole at 199 m.

Sedimentary context of the evaporite units

Throughout the formation evaporite rock and laminated grey siltstone and dolostone are associated (Figs 3 and 4; Bennett *et al*., 2016). The laminated siltstone may contain bivalves, spirorbids, ostracods, fish fragments and, more rarely, conchostracans, and may be burrowed or bioturbated. In many examples, there are no associated desiccation surfaces or other indications of emergence. By contrast, in the Glenrothes, East Dron and Norham boreholes, there are examples of desiccated horizons less than 1 m above layers of evaporite nodules.

Evaporite deposits occur in many beds in the Hoddom Borehole. They occur in thin and medium beds of dolostone, laminated units of siltstone, and in beds of fine-grained and very fine-grained sandstone. Some siltstone and sandstone beds are bioturbated and there are scattered ostracods, plant debris, fish fragments and the bivalves *Modiolus*, *Sanguinolites* and *Leiopteria* (Dean, 1997). Desiccation cracks and palaeosols are few, though the tops of some dolostone beds are brecciated.

By contrast, in the Norham core, 25 evaporite units are clustered in six packages, 3.57 to 5.74 m thick, of laminated grey siltstone, interbedded with beds of dolostone (Supplementary Data 2); for example, the 5.74 m thick association contains seven evaporite units (Figs 6 and 7). Each package overlies either a rooted palaeosol, or a bed of sandy siltstone of the type described by Bennett *et al*. (2016). At the top, the siltstone either passes up into ripple cross-laminated, very fine-grained sandstone, or is overlain sharply by fluvial, cross-bedded, fine-grained to medium-grained sandstone. Within a package, there are no clearly defined erosion surfaces, pedogenic or desiccated horizons. The siltstone underlying and overlying evaporite beds is burrowed and bioturbated in part, predominantly by the ichnotaxon *Chondrites* (Bennett *et al*., 2017). Though not abundant, ostracods

171 are the ubiquitous element of a low-diversity biota that also includes fish and plant debris, and the
172 bivalves *Modiolus* and *Naiadites*.

173 A thinner package, 3.14 m thick, includes a single nodular gypsum unit, 0.54 m thick, within
174 the upper part of the succession (Fig. 8D; Facies 3 below). The base is a thin, bioturbated sandy
175 siltstone that overlies a structureless grey siltstone with an irregular, brecciated top, interpreted as a
176 gleyed inceptisol (Kearsey *et al*., 2016). The lowest 2.3 m comprise plane-laminated dark grey
177 siltstone and composite dolostone units abundantly burrowed by *Chondrites*, ?*Zoophycos* and
178 subordinate phycosiphoniform trace makers along with the presence of *Naiadites* (Bennett *et al*.,
179 2017). The nodule bed hosted in dark dolostone containing abundant pyrite succeeds this. A unit of
180 laminated siltstone and dolostone containing sporadic selenite crystals 18 cm thick overlies this bed,
181 and the sharp base of a cross-bedded sandstone unit containing mudstone rip-up clasts and plant
182 fragments terminates the succession.

183 Grey and dark grey siltstone, either as separate beds or interlaminated, hosts the evaporites.
184 The grey siltstone is composed of normally graded laminae of angular to subangular quartz,
185 plagioclase, potassium feldspar, muscovite and clay minerals. The dark grey siltstone also contains
186 variable proportions of dolomite crystals, typically associated with amorphous organic matter (AOM)
187 and framboidal pyrite. There may be patches of poikilotopic anhydrite or gypsum cement in some
188 rocks.

189 Evaporites are also common in thin beds of ferroan dolostone (Fig. 3) that occur within the
190 successions of laminated grey siltstone. Many of these evaporite-bearing dolostones are composed
191 of planar-textured subhedral dolomite (Sibley & Gregg, 1987) with average rhomb sizes of 40 to
192 140 µm. By contrast, other beds are dense, dark dolomicrite, composed of <5 µm unimodal grains of
193 rhombohedral planar-e to planar-s dolomite. In some thin sections, spongy clotted fabrics are
194 apparent, but SEM analysis shows the clotted fabrics to consist of the finest grained dolomite and
195 little or no organic matter is present.

DESCRIPTION OF EVAPORITE FACIES

Table 1 summarizes the macroscopic and petrographic characteristics (Fig. 5) of 13 evaporite forms. Some forms occur singularly, whereas others associate in seven facies.

Facies 1: nodules hosted by siltstone and sandstone

Ovoid to subspherical and irregular nodules of gypsum or anhydrite, up to 15 cm diameter, within thinly laminated siltstone are the most common evaporite form recorded in the Midland Valley borehole logs (Figs 3, 8A and B). Many occurrences in the Glenrothes and East Dron boreholes lie up to about 1 m beneath desiccation surfaces or brecciated top surfaces of siltstone beds (Facies 1a). In examples of this type in the Norham core, sedimentary lamination is deformed around the nodules. By contrast, evidence for emergence, including desiccation cracks and brecciated sediment, is absent from boreholes in the west of the Midland Valley and the evaporite nodules occur in thick units of planar-laminated siltstone. Similarly, in the Hoddom core packages of siltstone and fine-grained sandstone, several metres thick, contain many irregularly bound, bedding-parallel layers of generally small nodules (<2 cm) (Facies 1b; Fig. 8C). Facies 1b nodules are typically concentrated becoming mosaic or chicken-wire forms and the nodule proportions may increase or decrease upwards.

Facies 2: nodular–laminated evaporite units

The Norham core contains nine complex units, 0.37 to 0.80 m thick, of associated protonodules, nodules, chicken-wire texture and anhydrite rock. All units are in the lower part of the formation, below the depth of 320 m. Anhydrite, commonly with porphyrotopic gypsum rims, is dominant in all but the uppermost example, which is replaced by secondary gypsum. Facies 2 does not occur in the Hoddom core or in any Midland Valley borehole. Two sub-facies are recognized (Fig. 9).

Five examples of Facies 2a (Fig. 9A) consist of a zone at the top of nodules set in dolostone, becoming chicken-wire textured downwards and passing abruptly into anhydrite rock. The matrix is siltstone within the chicken-wire and anhydrite rock zones. At the base, protonodules occur along lamination in dark grey siltstone, silty dolostone or dolostone. In two examples (421.33 to 421.70 m;

422.14 to 422.94 m), the various forms are separated by a few centimetres of laminated siltstone (Fig. 9A). A water-escape structure occurs at the top of the lower of the two examples. In the four examples of Facies 2b the zones are in reverse order (Fig. 9B).

The nodular zone consists of an accumulation of round, oval or elongate anhydrite masses, typically a few centimetres in diameter, and in some examples elongated vertically. The top of a Facies 2a evaporite unit at 377.61 to 378.25 m has a sharp contact with overlying siltstone. The chicken-wire zone is 0.15 to 0.20 m thick consisting of small (<5 cm) nodules, separated by small enclaves, smears and trails of siltstone or dolostone. The nodules are irregular in shape and appear flattened horizontally.

The anhydrite rock zone is 7 to 30 cm thick. In Facies 2a, the base, on siltstone or laminated dolostone, is sharp and in some examples bulbous. Trails of small, irregular, angular enclaves of siltstone matrix define a crude lamination that may be parallel to that in the sedimentary rocks beneath, or steeper where the enclaves have a sigmoidal shape. In part, the contact is stylolitic and trails of the enclaves outline former nodule boundaries (Fig. 8E). Granoblastic anhydrite characterizes this unit (Fig. 5E and F).

The uppermost example of Facies 2a (Fig. 9C) is composed mostly of sub-horizontal bands of vertically aligned selenitic gypsum containing few anhydrite inclusions, though zones of aphanitic anhydrite are preserved locally. Common enclaves of siltstone in trails testify to the original presence of the anhydrite rock zone. Satin-spar veins disrupt gypsum nodules at the top of the dolostone bed. The very thin lamination in the dolostone is contorted.

Protonodules of either anhydrite or gypsum are present in six examples of Facies 2, in the uppermost 10 to 30 cm underlying the anhydrite rock zone in Facies 2a or at the top of the succession in Facies 2b. The protonodules in Facies 2a are 1 to 20 mm diameter and aligned along the lamination, which is warped over them (Fig. 9A). The smaller nodules are typically round, oval or

lenticular in shape. Within siltstone or silty dolostone, dark, very thin laminae and discontinuous streaks of dolomite rhombs 1 to 5 µm across, typically underlie and overlie the protonodules. In the uppermost example of Facies 2a (Fig. 9C), the protonodules are composed of gypsum with anhydrite cores and extensive dolomite replacing the sulphate minerals. Here, the protonodules are hosted by laminated dark dolostone with crystal size 1 to 5 µm; paler lenticular zones of planar-e to planar-s crystals 8 to 25 µm, define the lamination. Scattered throughout are sporadic flakes of mica and irregular, corroded quartz; anhydrite and small patches of celestine fill pores in the finer-grained dolostone.

In Facies 2b, the protonodules at the top of the succession are mainly irregular discontinuous streaks along the lamination and in places resemble disrupted thin layers (Fig. 9B). The proportion of evaporite decreases abruptly upwards and there also appears to be a sharp base to the laminated siltstone.

Facies 3: compact gypsum nodule beds

Facies 3 occurs in the Norham core but not in Hoddom or elsewhere. The Norham core contains one unit, 0.54 m thick, with its base at a depth of 182.96 m. It comprises two beds of close-packed, round gypsum nodules, up to 1 cm across, in a dolostone matrix (Fig. 8D); a few nodules are elongate and aligned vertically. Many millimetre-wide sub-horizontal gypsum veins cut the unit. Laminated dolomicrite, 2 cm thick and containing tiny clotted aggregates and wispy steaks of organic matter separates the beds. Palynological preparation shows this to include fragments of thin sheets of AOM.

The dolostone matrix is composed of unimodal, planar, 1 to 5 µm dolomite crystals. Irregular, discontinuous dark laminae, up to 100 x 6 µm, are rich in 5 to 35 µm pyrite framboids, and clusters and trails of associated pyrite spherules up to 1 µm in diameter. The very fine pyrite outlines straight and curved rods, larger oval forms and a mesh of interlinked tube-like structures entwining sporadic mica and highly corroded quartz grains, and pyrite framboids (Fig. 10E and F). The pyrite

layers also locally contain randomly orientated anhydrite laths up to 10 µm long, and pore and vein-like fills of celestine. EDX spot analyses of the celestine show that it contains small amounts of Ba.

Facies 4: evaporite – dolostone/ siltstone laminites

This facies is commonest in the Hoddom core where there are seven examples (Supplementary Data 3); descriptions of three of these illustrate the variation. Firstly, a 26 cm thick laminated bed of very fine-grained quartz sandstone with its base at 166.74 m occurs between dolostone beds containing nodular anhydrite. Evenly distributed throughout the sandstone are aggregates up to 3 mm across of aphanitic anhydrite; many of the aggregates resemble the equant lozenge-shaped form of gypsum (Fig. 5A). The cement is granular to poikilotopic anhydrite. Secondly, at 168.93 to 169.08 m laminated siltstone, very fine-grained sandstone and discontinuous layers of dolomicrite with opaque streaks are packed with lozenge-shaped aggregates up to 0.5 mm of aphanitic anhydrite (Fig. 5B). The shape of the anhydrite aggregates again resembles gypsum. Thirdly, a 20 cm thick bed with its base at 171.21 m is composed of laminated, very fine-grained sandstone, anhydrite rock and lenticular remnants of sandy siltstone. The anhydrite rock contains grains of quartz and feldspar with intricate margins and some pyrite. The sandy siltstone is composed of quartz, mica and feldspar grains, along with sporadic wood fragments, in a supporting matrix dominated by finer grained mica/illite; anhydrite heavily impregnates the sandy siltstone.

A single example of Facies 4 occurs in the Norham core at 450.50 to 451.14 m (Figs 6 and 7E). This consists of convolute-bedded dolostone, siltstone, claystone and laminated anhydrite rock. Interleaved with these are laminae of siltstone and anhydrite that alternate on a millimetre to sub-millimetre-scale (Fig. 7E). The anhydrite laminae are aphanitic with grains up to 20 µm and intergrown with single crystals and irregular aggregates of planar-e dolomite with an average crystal size of 7 µm; thicker laminae are coarser grained and granoblastic. In the convoluted upper part of this unit, the intercalated brown claystone occurs in ragged and disrupted strips impregnated with anhydrite (Fig. 10C and D). The claystone contains thin sheets of carbonaceous matter, along with

295 quartz and hornblende grains and randomly orientated mica plates, in a muscovite/illite groundmass
296 containing minute pockets of anhydrite.

297 ### Facies 5: dolostone–evaporite facies

298 Gypsum and/or anhydrite masses commonly occur solely within ferroan dolostone beds. The
299 proportion containing evaporite masses varies from about 5% in the Deaconhill Borehole (5 out of
300 94) to 16% in Loch Humphrey (20 out of 126); there are just two occurrences in Barnhill (out of 82
301 dolostones) and no record in the Ascog and Knocknairshill boreholes. Facies 5 is more common than
302 Facies 1 in the Loch Humphrey borehole, but less so in East Dron. In the Glenrothes Borehole
303 dolostone beds containing evaporite minerals have a more widespread distribution than Facies 1
304 (Fig. 3).

305 In the Norham core, 21 of 272 dolostone beds contain gypsum or anhydrite. The evaporite
306 forms occur as sporadic disseminated crystal aggregates, void fills, irregular angular forms (Fig. 7F) or
307 coalescent masses of round nodules. Laminated evaporite rock occurs at the base of a few beds
308 alternating with dolostone on a millimetre-scale (Fig. 7F). The host dolostone is typically a mosaic of
309 40 to 140 µm unimodal to polymodal planar-s rhombs. Sporadic shell fragments, mainly ostracods,
310 bioturbation and framboidal pyrite may be present. Scattered angular silt grains of quartz with
311 highly irregular margins are present in many of the dolostone beds. A few beds display lamination,
312 marked by layers of differing average grain size; the lamination is typically deformed around the
313 margins of the nodules. Round patches of coarser dolomite are also present. Some of the dolostones
314 are composed of dense dolomicrite <5 µm with opaque matter forming a spongy, clotted texture,
315 streaky masses and discontinuous thin lenses. A water escape structure occurs at the top of one of
316 these beds (Fig. 8F).

317 In the Hoddom core 62 of 117 dolostone beds contain anhydrite and/or gypsum as layers of,
318 or dispersed, protonodules, nodules, mosaic-nodular and chicken-wire masses. Evaporite forms
319 comprise up to as much as 75% of beds, though there are a few beds up to 15 cm thick of anhydrite

rock containing trails of dolomicrite or siltstone. Nodules may be concentrated at the top or base of beds and the proportion both increases and decreases towards the top of many beds.

Facies 6: residue beds

Small-scale evidence of the probable former presence of evaporite deposits is present in the upper part of the Norham core, within 50 m of the present-day surface. Here, two bedding-parallel zones a few centimetres thick are composed of spongy calcite networks; some of the calcite present may be pseudomorphous after gypsum. Residue beds have not been reported from any Ballagan Formation exposure.

Facies 7: pseudomorphs after halite

Halite (*sensu strictu)* has not been recorded from the Ballagan Formation, but its former presence has been noted from euhedral pseudomorphs of siltstone or fine-grained sandstone in Chattlehope Burn (Cater *et al*., 1989) and near Langholm (Leeder, 1974). In addition, the logs of the Loch Humphrey, East Dron and Glenrothes boreholes (Fig. 3) record the presence of pseudomorphs up to 5 mm, some preserving hopper faces within units of laminated grey mudstone. In the Glenrothes and East Dron boreholes, the pseudomorphs occur up to about 1 m beneath desiccation crack horizons or dolostone beds. This facies has not been found in the Norham or Hoddom cores.

INTERPRETATION

The mineralogy and textures of ancient evaporite rocks relate to a history of multiple replacements following deposition, burial and later exhumation (e.g. Murray, 1964; Schreiber & El Tabakh, 2000; Warren, 2006). Despite this, the Ballagan Formation rocks contain convincing petrographic evidence that the primary evaporite mineral was gypsum. Lenticular pseudomorphs composed of aphanitic anhydrite aggregates and having the prismatic shape typical of gypsum occur in the evaporite laminites, among the small nodules, and at the margins of some larger nodules (Fig. 5A, B and D). A general diagenetic sequence from primary gypsum to anhydrite to secondary gypsum is inferred from the mineralogy and textural relationships present (Table 2). This is broadly compatible with the

scheme interpreted from the Jurassic Purbeck evaporites in southern England by West (1964). Understanding the main features of the diagenetic history is important in interpreting the facies.

Facies 1: Nodules hosted by siltstone and sandstone

The two subfacies have distinct origins. The large nodules in Facies 1a grew by the accretion of gypsum crystals, progressively displacing host sediment from the mass and deforming the lamination (Fig. 5D). Examples of nodules in the Glenrothes and Norham cores arranged as sinuous strings fit the description of enterolithic veins (e.g., Fig. 8B). Their occurrence up to 1 m beneath a brecciated siltstone or a desiccation crack horizon suggest that the nodules grew in the vadose or shallow phreatic zone beneath the floodplain through evaporation. This is like many Holocene supratidal sabkhas (Warren, 2006 and references therein).

The generally smaller nodule concentrations of Facies 1b in the Hoddom cores cannot be related to a contemporary ground surface and the host rocks suggest uninterrupted deposition in standing water bodies. The evaporite textures exhibited are similar to those described for gypsum mush accumulations in ponds and lagoons associated with some of the Persian Gulf sabkhas (e.g. Butler *et al*., 1982). These nodule layers in Hoddom are interpreted as having formed during dehydration of a gypsum mush, a mechanism proposed by Warren & Kendall (1985). The repeated beds of gypsum mush and siliciclastic sediment imply swings between episodes of desiccation and wetter conditions that provided sediment input into the water body. The evaporite nodules in boreholes from the north and west of the Midland Valley probably also formed in this way.

Facies 2, 3, 5: association of dolostone with evaporite rock

The strong link between evaporite rock and dolostone in the Ballagan Formation was ascribed to a floodplain saline – hypersaline facies association by Bennett *et al.* (2016). Dolostone beds are characteristic of Facies 2, 3 and 5, but are also a more widespread feature of the Ballagan Formation and not all contain evaporite nodules. Some of the dolostones may have a palustrine origin, similar to those for example in the Upper Cretaceous Leza Formation (Suarez-Gonzalez *et al.*, 2015) or the

upper Mississippian strata of Kentucky (Barnett *et al.,* 2012). However, the Ballagan evaporite-bearing dolostones do not show the pedogenic features of those from Kentucky. The formation of gypsum in palustrine carbonates is favoured by a semi-arid climate (Platt & Wright, 1992; Alsonso-Zarza, 2003) or where dolomite dominates (Sanz-Rubio *et al*., 1999).

The evaporite-bearing Ballagan dolostones composed of planar-s dolomite with average rhomb sizes of 40 to 140 μm are likely recrystallized. By contrast, the dark dolomicrites, with rhombohedral grains <5 μm are considered to be either primary precipitates, or more probably, early replacements of precursor very high magnesium calcite (Vasconcelos & McKenzie, 1997; Warren, 2000; Gregg *et al*., 2015). The formation of primary dolomite has long been regarded as difficult, though Pierre *et al.* (1984) argued that finely crystalline dolomite is precipitated penecontemporaneously with gypsum in the Ojo de Liebre lagoon in Baja California. However, photosynthetic and chemotrophic microorganisms have been shown to have a role in dolomite nucleation, both from experimental and field studies (e.g. Vasconcelos & McKenzie, 1997; Wright & Wacey, 2005; Barbieri *et al.*, 2006; Mastandrea *et al*., 2006; Bailey *et al*., 2009; Sánchez-Román *et al*., 2009; Bontognali *et al.*, 2010; Bahniuk *et al*., 2015).

The association in modern examples of dolomite and evaporite deposits with microbial mats is well known (e.g., references above; Warren, 2010 and references therein). By contrast, in ancient deposits these organic structures are generally not preserved. However, Schieber (1999, 2007) described a range of characteristic sedimentary indicators that point to the probable former presence of microbial mats. No bioherms have been recorded from the Ballagan Formation, but of those indicators mentioned by Schieber the following are present. They are dark, crinkled, discontinuous carbonaceous laminae in dolostone and siltstone associated with evaporite protonodules; ragged ends to strips of siltstone; thin films of clay minerals with tiny pyrite aggregates draping 8 to 25 μm dolomite crystals within dolostone; trails of fine pyrite in dolostone;

394 grains of ragged quartz floating in dolostone; and randomly orientated micas within dolostone (Fig.
395 10A to F).

396 ### Facies 2: Nodular – laminated evaporite units

397 Superficially, Facies 2 resembles classic marine-marginal sabkha cycles of the Persian Gulf as
398 described by Shearman (1966, 1978) and Kendall (1984) and related by Kirkham (1997) to
399 transgressive – regressive sea-level cycles. In this model, the identification of three main features is
400 critical. These are laminated marine mudstone associated with microbial mats at the base commonly
401 with gypsum crystals; displacive nodular and chicken-wire evaporites and enterolithic structures
402 within the overlying siliciclastic or carbonate sediment; and an erosion surface at the top (Shearman,
403 1966, 1978; Kendall, 1984; Kirkham, 1997; Schreiber & El Tabakh, 2000).

404 The thickness of examples of Facies 2 fall within the typical range of sabkha cycles of 30 cm
405 to 2 m (Schreiber & El Tabakh, 2000). However, the marine and intertidal deposits are substituted by
406 planar laminated siltstone and interbedded dolostone deposited within bodies of standing water,
407 most likely coastal plain lakes (Bennett *et al*., 2016). However, the presence of single tier *Chondrites*
408 burrows, implying short duration occupation by marine ichnotaxa, suggests that marine water
409 recharged these lakes during storm events (Bennett *et al*. 2017).

410 Laminated siltstone and dolostone host evaporite protonodules at the base of Facies 2a.
411 Though the organic content of these rocks is now low, there are features strongly suggesting the
412 growth of evaporite nodules within microbial mats. This includes the undulating form of thin layers
413 of dark (<5 µm) and light (8 to 25 µm) dolomicrite, in some cases confining the trails of
414 protonodules, along with very thin laminae of clay minerals associated with pyrite and isolated
415 grains of quartz or feldspar (Fig. 10A and B). The coarser Fe-bearing (EDX) dolomite crystals are
416 compatible with growth during bacterial fermentation diagenesis as the sediment was buried (Irwin
417 et al., 1977; Irwin, 1980; Mastandrea *et al*., 2006). If so, then this dolomite implies a high original
418 organic content. Though microbial mats are an important element of the intertidal zone of marine

marginal sabkhas, they also occur at the margins and on the floor of shallow lakes, among other environments (Warren, 2006 and references therein).

Silt from runoff or from floods then buried the microbial mats. Evaporation led to the shallowing of the lake, hypersalinity and finally to deposition of dolomicrite. At this stage, the lakebed may have been the top of the dolostone, though a brecciated or cracked top to suggest subaerial exposure was not identified in any of the examples examined. A water-escape structure (Fig. 9A) is cited as evidence of exposure. Gypsum nodules then formed within the silt and dolomicrite during further evaporation and lowering of the water table. In the sabkha model this should have led to uplift and erosion (Shearman, 1978), but erosion surfaces are difficult to prove in core in the absence of a regolith which is not present in any examples from the current study.

The nodular and chicken-wire anhydrite in the Norham core are dominated by aphanitic, felted-lath and related textures which Shearman & Fuller (1969) and Holliday (1973) considered to represent two generations of syndepositional anhydrite formation, rather than dehydration caused by burial (Murray, 1964). At the margin of some nodules, the lozenge-shaped pseudomorphs after gypsum are composed only of aphanitic anhydrite (Fig. 5D). Where these coalesce into nodules coarser, felted-laths surround the aphanitic ‘cores’ and, as proposed by Holliday (1973), resulted from the precipitation of anhydrite without a gypsum precursor. This interpretation implies either an increase in salinity of the enclosing brine as the temperature rises, or that the brine was at first saturated with respect to gypsum but underwent further concentration and rise in temperature to reach anhydrite saturation (Hovorka, 1992).

Progressive growth and compaction of the nodules reduced the volume of interstitial sediment from a continuous interstitial mass in the nodular zone, to discontinuous streaks and thin films in the chicken-wire zone and to trails of tiny detached enclaves defining a weak lamination in the anhydrite rock zone. The presence of trails of siltstone that define the margins of well flattened nodules (Fig. 8E) seems to preclude the conversion of siva-twinned gypsum growths to anhydrite

444 nodules along the lines proposed by Shearman (1985). Siltstone always hosts the anhydrite rock
445 zone and its low permeability would impede the escape of water released by the dehydration
446 reaction, allowing extreme compaction (Shearman & Fuller, 1969). The retention of sulphate-
447 saturated fluid in the siltstone may have promoted anhydrite grain growth and granoblastic texture.
448 This contrasts with the nodular and chicken-wire zones, hosted by dolostone that may have lithified
449 early, as suggested by the 3D preservation of plant stems in some non-evaporite-bearing examples
450 (Scott & Meyer-Berthaud, 1985).

451 In Facies 2b (Fig. 9B), the sharp top to the chicken-wire zone is interpreted to be the eroded
452 sabkha surface beneath which the evaporite rocks formed. The nodular and chicken-wire anhydrite
453 zones are reversed only because their host is reversed. No microbial mat developed. The laminated
454 siltstone at the top of the succession represents renewed flooding and sedimentation of silt and
455 gypsum laminites that were disrupted during dehydration to anhydrite.

456 ### Facies 3: compact gypsum nodule beds

457 The co-existence of nodular evaporite with dark dolomicrite containing abundant pyrite from the
458 Norham core is the only example known in the Ballagan Formation. The pyritized tube-like forms
459 (Fig. 10E and F) suggest a filamentous microbial origin. The detrital quartz and mica grains appear
460 entwined within these structures, a feature of microbial mats demonstrated experimentally by
461 Frantz *et al*. (2015). The preservation of pyrite framboids with dolomite indicates that the
462 mineralization occurred during or shortly after sediment deposition, rather than during burial, and
463 furthermore suggests the involvement of sulphate-reducing bacteria. Vasconcelos & McKenzie
464 (1997) described microbially-mediated dolomite in a layer of hypersaline black sludge just above the
465 sediment-water interface from Lagoa Vermelha in coastal Brazil; Wright & Wacey (2005)
466 demonstrated this experimentally in the Coorong, Australia. The further presence of interstitial
467 anhydrite and celestine emphasizes microbial involvement (Taberner *et al*., 2002; Sanz-Montero *et*
468 *al.,* 2009). The processing of organic matter by bacteria in this zone locally causes high alkalinity, a

469 requisite for the precipitation of dolomite (Wright & Wacey, 2005; Sánchez-Román *et al.*, 2009). In
470 Facies 3 corroded quartz grains suggest that alkaline conditions prevailed. The relatively large size of
471 the framboids implies that the environment was dysoxic (Wilkin *et al*., 1996; Bond & Wignall, 2010).

472 The facies occurs near the top of a sedimentary succession that began with a flooding event
473 and subsequently dominated by suspension sedimentation in a body of standing water. Much
474 reduced sediment input allowed establishment of a marsh. The evaporite beds formed within the
475 putative microbial mat before lithification, as indicated by the deformation of the mat (Fig. 10E),
476 following further flooding and burial of the mat.

477 ### Facies 4: evaporite – siltstone/sandstone laminites

478 Localized thin units (Figs 6, 7E and 8G) of alternating laminae of evaporite rock and clastic or
479 carbonate rock represent direct sedimentation of gypsum into a brine pool; pseudomorphs after
480 gypsum from the Hoddom core illustrated in Fig. 5A formed within the sandy substrate of the pool.
481 The successions of alternating laminae may represent seasonal sedimentation. The equigranular
482 aphanitic anhydrite is texturally distinct from that of the nodules and is compatible with a precursor
483 as fine-grained gypsum deposited from spontaneous 'whitings' (Babel, 2004) during episodes of
484 rapid evaporation. By contrast, the clastic laminae resulted from the influx of silt and immature fine
485 sand during wet periods or possibly as aeolian deposits (Gunatilaka & Shearman, 1988). Thicker
486 evaporite laminae within the succession could be the result of seasonal mixing or of longer arid
487 periods (Babel, 2004). Though the scale of the thinnest laminae is compatible with annual
488 accumulations (varves; Einsele, 2000), Warren (2006) warned that, rather than annual, such
489 lamination may have resulted from repeated flooding events. Flooding events generating sandy
490 siltstones were characteristic of the Ballagan coastal plain according to Bennett *et al.* (2016) (Fig. 4).
491 The clastic laminae in one of the Hoddom examples have features of sandy siltstone deposited in
492 shallow water.

493 The characteristics of the brown claystone strips within the upper part of the deformed unit
494 in the Norham core (Figs 7E, 10C and D) suggest that these are relicts of a microbial mat. Indirect
495 evidence following Schieber (1999, 2007) includes the ragged form of the strips interleaved with
496 anhydrite, randomly orientated clays and micas, dispersed corroded quartz and hornblende grains
497 and the thin discontinuous sheets of carbonaceous matter. Soft-sediment deformation of the whole
498 unit is probably contemporaneous with dehydration of primary gypsum to anhydrite and may have
499 been the cause of mat rupture.

500 ### Facies 5: dolostone – evaporite facies

501 Though in many of the dolostones the dolomite has recrystallized, a few examples of primary
502 dolomicrite remain. The presence of interlaminated dolostone and evaporite at the base of some
503 dolomicrite beds (lower part; Fig. 7F) containing dispersed, irregular nodules throughout suggests
504 that the evaporite formed penecontemporaneously with the dolomite in a shallow hypersaline lake
505 or brine pan. Penecontemporaneous crystallization of dolomite and gypsum has been inferred to
506 occur in the coastal salinas of Baja California (Pierre *et al.*, 1984). By contrast, the coalescent,
507 rounded nodules seen in other examples formed above the water table following drying out of the
508 lake, as envisaged for Facies 2a. The water-escape structures in these beds probably resulted from
509 the expulsion of water produced during dehydration of gypsum.

510 ### Facies 6: residue beds

511 The residue beds formed through dissolution and carbonate replacement of the evaporites,
512 probably in the near subsurface during Cenozoic or, more recent, uplift. The original bed thickness of
513 these examples was probably insufficient for collapse to have taken place. However, collapse breccia
514 has been illustrated from post-Tournaisian strata in the Lyne Formation near Bewcastle in the
515 Northumberland Basin (Ward, 1997, fig. 4a).

Facies 7: pseudomorphs after halite

Displacive halite cubes are a feature of marine marginal sabkhas and salinas, forming at, or a little above, the groundwater table through capillary evaporation (Schreiber & El Tabakh, 2000). A similar origin is inferred for the sporadic occurrences in the Ballagan Formation.

DISCUSSION

Ancient evaporite facies are rarely preserved in surface exposures and the immediate subsurface in non-arid regions because of dissolution. Their former presence in exposures of the Ballagan Formation had been recognized from calcite pseudomorphs in some dolostone beds at Burnmouth (Scott, 1986). Furthermore, exposures containing satin spar veins are characteristic only of this formation in the Mississippian succession of the region (Hall *et al*., 1998; Monro, 1999). However, the importance of evaporites as an integral part of the depositional regime is only apparent through subsurface investigations.

The coastal floodplain model for the Ballagan Formation proposed by Francis *et al*. (1970), Anderton (1985) and Andrews *et al.* (1991) has been developed further by Bennett *et al*. (2016, 2017) and Kearsey *et al*. (2016). Scott (1986) proposed an alternative palaeogeography from studies at Burnmouth (Fig. 1). He postulated that the evaporite rocks formed in sabkhas around the margins of a continental lake. Although there may be some examples of this environment, it is unlikely to be the primary setting, given the sporadic occurrences of storm-derived marine invertebrate fossils across the Midland Valley and the proximity of brachiopod and crinoid-bearing limestones of the partly coeval Lyne Formation in the adjacent Northumberland – Solway Basin (Fig. 2; Leeder, 1975; Waters *et al*., 2011). The 128 cryptic marine intervals in the Norham core, comprising a storm-derived *Chondrites* ichnofacies and scolecodonts demonstrate abundant marine flooding into the Tweed Basin (Bennett *et al.,* 2017). The restricted evaporite mineralogy of dolomite, gypsum and anhydrite along with trace amounts of celestine and barite is more typical of marginal marine than of continental deposits (Warren, 2006; Chagas *et al*., 2016).

Gypsum $\delta^{34}S$ values of 20‰ from the Ballagan Formation in the Midland Valley reported by Pattrick *et al*. (1983) are close to Tournaisian seawater $\delta^{34}S$ values of 21±1‰ (Kampschulte *et al*., 2001). However, the two Ballagan analyses quoted by Pattrick *et al*. (1983) are likely to have been from satin spar veins as the samples were from exposures. Therefore, the values quoted may not support the marine origin of the sulphate, because the sulphur isotopes will have undergone fractionation as a result of phase transformation during burial and uplift (Taberner *et al.*, 2002), though the effect of this is often regarded as small (Schreiber & El Tabakh, 2000). More compelling evidence for the origin of the sulphate is provided by the repeated cryptic marine flooding events (Bennett *et al*., 2017).

The interpretation here is that Ballagan evaporites formed because of the evaporation of shallow hypersaline lakes. The coastal plain model for the Ballagan Formation (Fig. 12) contains open and closed saline lakes (Bennett *et al*., 2016, 2017), along with meteoric-fed fresh and brackish water lakes (Williams *et al*., 2006). The current study envisages that some of the closed, marine-fed saline lakes episodically evaporated to become hypersaline, depositing gypsum. The juxtaposition of lakes with differing salinities is seen today in the Brazilian Pantanal wetlands (Costa *et al*., 2015), though this setting is not coastal. Many lakes were probably temporary and short lived, though along the margin of the Northumberland – Solway Basin some may have been semi-permanent, as in the Hoddom area. Similar bodies of water probably existed to the west of Glasgow. Marine and freshwater surface flooding events formed and recharged the lakes. Microbial mats developed along some lake margins and perhaps the floors during early stages of a lake's existence. The record of evaporite occurrences across the region (Fig. 1) shows particular concentrations to the western extent of the Midland Valley, at Glenrothes and near Perth in the east, in the Northumberland – Solway basin, and in the Tweed basin. These locations probably reflect ready access for marine floodwaters during short-lived storm surges, or through marine water intrusion through the substrate. Here, there is greater evidence for extensive sabkha adjacent to the lakes, where

evaporation led to the growth of gypsum nodules or, in some localities halite cubes, in the floodplain silts.

The preservation of evaporites during the wet season probably resulted from several factors. The common occurrence of cohesive debris flow deposits (Bennett *et al*., 2016) and the formation of temporary lakes during tropical rainfall events suggest high surface runoff over the low permeability floodplain. This may have resulted in only small dilution effects on the sulphate-saturated groundwater mass beneath the floodplain. Storm surges recharged perennial lakes with saline water. Sediment deposited during the wet season buried existing surfaces and added to lacustrine successions. Some of the perennial lakes may have been meromictic. This was possibly the case, for example, for deposition of the evaporite – siltstone laminites of Facies 4; laminated sediments are characteristic of many meromictic lakes (Babel, 2004). It is also possible that the evaporites formed during drier decadal or longer intervals which promoted preservation; no assessment has been published yet of climate rhythms within the region during the Tournaisian.

Tournaisian evaporites

Tournaisian evaporites are widespread in the palaeoequatorial British Isles and are also characteristic in successions from regions that would have been in close proximity, including eastern Canada. Farther afield, in mainland Europe (including Belgium and Poland), Central Asia (Kazakhstan) and the western North America, Tournaisian evaporites are associated with carbonate successions.

In the British Isles, the thickest succession occurs in the centre of the Northumberland–Solway Basin, where 1153 m of anhydrite-bearing strata were proved in the Easton No 1 Well, north of Carlisle (Fig. 1; Ward, 1997). Within the succession of carbonate rocks and mudstone about 120 anhydrite beds range from 30 cm to 7.9 m thick. Though Ward (1997) correlated the uppermost part of the anhydrite succession with the upper Chadian – lower Arundian Bewcastle Member of the Lyne Formation, the age of the lower part, which contains some of the thickest evaporite units, is not well constrained biostratigraphically and probably extends down into the Tournaisian. Ward (1997)

591 considered subaqueous gypsum deposition in salinas as the likely origin for the Easton anhydrite
592 beds. However, thickness of units and inferred widespread subcrop (Fig. 1) suggest that these might
593 be marine deposits. To the east, the occurrence of barite within Permian rocks adjacent to the
594 Ninety Fathom Fault east of Newcastle and of brine flow into historic coal mine workings might
595 suggest that the areal extent of these evaporites is even greater than suggested by Ward (Younger *et*
596 *al.,* 2016).

597 To the south, in Cumbria, thin beds of gypsum are associated with limestone in the Marsett
598 Formation (Rose & Dunham, 1977) and breccias in the Pinsky Gill Formation at the western end of
599 the Stainmore Basin may have formed through gypsum dissolution (Holliday *et al*., 1979). On the
600 southern flank of the Askrigg Block in North Yorkshire, 26 m of laminated anhydrite, dolostone and
601 dolomitic siltstone were proved in the Cominco S2 borehole (Fig. 1, Supplementary Data 1;
602 Arthurton *et al*., 1988). In Derbyshire, 74 m of the upper Tournaisian Middleton Dale Anhydrite
603 Formation were proved in the Eyam Borehole (Dunham, 1973; Strank, 1985). The formation consists
604 of thinly interbedded dolostone, mudstone and anhydrite rock, the last lithotype comprising 45% of
605 the thickness. The thinly interbedded character of the anhydrite rock and dolostone likely represents
606 shallow, marginal marine environment during onlap of the Derbyshire High (Gutteridge, 1987). On
607 the Hathern shelf and in the Widmerpool gulf between Derby and Loughborough, at least 97 m of
608 nodular evaporite rock within a limestone-dolostone-mudstone succession of the Tournaisian
609 Hathern Anhydrite Formation were proved in the Hathern No. 1 Borehole (Llewellyn & Stabbins,
610 1970) and in the Long Eaton No. 1 Borehole (Fig. 1; Supplementary Data 1). Here, Llewellyn &
611 Stabbins (1970) and Carney *et al*. (2001) envisaged deposition in sabkhas.

612 In the south of Ireland, Famennian to Tournaisian times saw a diachronous marine
613 transgression north-eastwards on to non-marine strata of ‘cementstone’ facies (Clayton & Higgs,
614 1979; Clayton *et al*., 1986; Pracht & Somerville, 2015). Evaporites were proved in the subsurface in
615 the Lough Allen Basin south-west of Enniskillen and near Killeshandra on the margin of the south-

616 west limit of the Longford-Down Massif (Sheridan *et al*., 1967; Clayton & Higgs, 1979; Mitchell, 1992;
617 Philcox *et al*., 1992; Waters *et al*., 2011). North-west of Lough Neagh, near Draperstown, the
618 Tournaisian to earliest Chadian Altagoan Formation contains evaporite rocks within the 250 m of
619 peritidal sandstone, siltstone and stromatolitic limestone (Owens *et al*., 1977; Mitchell, 1997).

620 On the south side of Belfast Lough, beds and nodules of calcified evaporite occur within the
621 Ballycultra Formation, a succession of about 140 m of siltstone interbedded with thin beds of fine-
622 grained sandstone, dolostone and stromatolites (Griffith & Wilson, 1982; Clayton, 1986). A short
623 distance to the north, the Belfast Harbour Borehole (Fig. 1) penetrated 199.5 m of thinly
624 interbedded dolostone, limestone, evaporite rock and siltstone; anhydrite comprises 19% of the
625 thickness, occurring in beds less than 1 m thick and as masses within dolostone beds (Smith, 1986).
626 The presence of ?*Sanguinolites*, *Serpula*, algal framework detritus and structureless micritic pellets
627 were inferred by Smith (1986) to indicate deposition in shallow marine or lagoonal environments.

628 Along the southern margin of Laurussia in eastern Canada, Tournaisian cementstone facies
629 in the Maritimes Basin, similar to the Ballagan Formation, include halite, gypsum, anhydrite and
630 glauberite in the upper part of the Albert Formation (Horton Group) in New Brunswick (Carter &
631 Pickerill, 1985), the same unit that in Nova Scotia hosts significant tetrapod fossils (Anderson *et al*.,
632 2015). The disseminated sulphates, in part replaced by calcite, are associated with an evaporitic
633 lacustrine lithofacies comprising 'shale', siltstone and dolostone. However, these evaporites are on a
634 smaller scale than the Visean Windsor Group in Nova Scotia that contains several hundreds of
635 metres of evaporite deposits (Gibling *et al*., 2008).

636 Other equatorial evaporites from this time are not from coastal wetlands. On the southern
637 margin of the Brabant Massif in Belgium, dolostone at the top of the Engihoul Formation is strongly
638 karstified with depressions up to 15 m deep, and cavities filled with calcite replacements of selenitic
639 gypsum growths and intercalations of crinoidal rudstone (Poty, 2016). In the Pomeranian Basin of
640 NW Poland to the east, anhydrite beds and nodules are associated with black 'shale' and calcareous

claystone of the upper Tournaisian Grzybowo Formation, deposited in a restricted lagoonal environment within a carbonate shelf setting (Matyja, 2008). A similar shallow marine and lagoonal setting in the Baltic region produced a succession of carbonate rocks with gypsum and siliciclastic rocks (Witzke, 1990). To the east, the passive margin of the separate continent of Kazakhstan hosted a platform-carbonate succession that contains substantial evaporite deposits (Alexeiev *et al*., 2015).

On the equatorial western margin of Laurussia, from North Dakota to Alberta and Manitoba, strata laid down in the Williston Basin and Prophet Trough contain nodular and massive anhydrite, halite and dolostone deposited in late Tournaisian times (Stott & Aitken, 1993; Petty, 2010). These evaporites formed in an arid, marginal marine to supratidal sabkha setting during sea-level regression (Petty, 2010).

Climate implications

Modern coastal evaporite deposits are characteristically associated with arid or semi-arid climate zones, but also occur in seasonally wet tropical biomes (Warren, 2006, 2010; Ziegler *et al*., 2003). Evidence cited recently from the Ballagan Formation suggests a tropical, seasonal coastal wetland environment, thus conflicting with previous climate conclusions based on the evaporites alone. No aeolian deposits are known from the Ballagan Formation, but in a succession of dominantly fine-grained rocks, recognition would perhaps be difficult. More significantly, Kearsey *et al*. (2016) described a diverse suite of palaeosols that indicate a floodplain wetland rich in habitats ranging from forest to marsh. Using soil geochemical proxies Kearsey *et al*. (2016) determined estimates of mean annual rainfall of 1000 to 1500 mm, typical of equatorial zones. By contrast, abundant mudcrack horizons, the presence of deep vertic cracks in some of the palaeosols and variable soil alkalinities attest to high rates of evaporation, episodic drying out and periods of alternating wetting and drying in a strongly seasonal climate. This regime is further supported by the form of tree growth rings from woody plants recovered from Ballagan Formation sites in SE Scotland which Falcon-Lang (1999) likened to extant araucarian conifer wood from seasonal equatorial

environments. Moreover, dense lycopsid forests and swamps in the Albert Formation (Horton Group) of New Brunswick, and coal mires in the upper Tournaisian Price Formation of Virginia, are evidence of other wetlands that lie along the equatorial Laurussian margin at this time (Kreisa & Bambach, 1973; Falcon-Lang, 2004; Rygel *et al.*, 2006).

Bennett *et al*. (2016) interpreted the many thin beds of sandy siltstone that are distributed through the Ballagan Formation as cohesive debris flow deposits generated during frequent flooding events, thus lending further support for seasonal events. The sandy siltstone beds are significant in that they preserve associated tetrapod skeletal elements, along with other vertebrate, invertebrate and plant fossils. These beds overlie desiccated substrates and palaeosols and the floodwaters may have resulted directly from precipitation, though overbank flooding caused by hinterland rainfall is also a possible source. The presence of charcoal in these beds suggests wild fires; a feature of the present-day equatorial seasonal biome. The many thin beds containing short residence colonizations of *Chondrites* trace makers provides evidence for episodic marine flooding (Bennett *et al*., 2017). Although the role of eustatic sea-level rises cannot be ruled out entirely as a cause of the flooding, it is more likely that this is related to storm surges in the monsoonal climate regime in the Tournaisian of the region envisaged by Wright (1990) and Falcon-Lang (1999).

Bennett *et al.* (2016) and Kearsey *et al.* (2016) interpreted the Ballagan coastal floodplain to have been covered by a mosaic of juxtaposed sedimentary environments hosting vegetated and aquatic habitats. These were subject to change through seasonal flooding events. Tetrapods inhabited both the vegetated floodplain and floodplain lakes (Clack *et al.,* 2016). The hypersaline lakes and sabkhas interpreted from the abundant evaporite deposits increase the diversity of habitats present on the floodplain though these would have been challenging ones for vertebrate animals. These Ballagan environments developed following the mass extinction events at the end of the Devonian (Kaiser *et al*., 2015), when vertebrate terrestrialization in the Tournaisian accompanied

690 a change in the terrestrial flora that led to a new fluvial and floodplain architecture (Davies &
691 Gibling, 2013).

692 Fragmentation of the southern margin of Laurussia in early Tournaisian times formed a
693 gateway linking the Palaeotethys and Panthalassa oceans and established a monsoonal regime over
694 northern Britain, Nova Scotia and adjacent areas (Wright, 1990; Falcon-Lang, 1999). The formation
695 of evaporites at this time, and in particular the thick succession in the Northumberland – Solway
696 Basin (Ward, 1997), is a direct consequence of this continental juxtaposition. An analogous but
697 larger scale example are the halite and anhydrite deposits that formed on the equatorial margins of
698 Brazil and Africa during initial opening of the Atlantic Ocean in Aptian times. Using fully coupled
699 ocean-atmosphere models Chaboureau *et al.* (2012) showed that high salinity and aridity developed
700 despite the equatorial location. Ziegler *et al.* (2003) noted that during Mesozoic and Cenozoic
701 evaporite deposition coincided with seasonal climates, and juxtaposed with coal-forming
702 environments because the continental configuration lead to the existence of shallow, extensive
703 tropical seas and restricted basins.

704 Today, coastal wetlands with a strongly seasonal climate occupy more than two-thirds of the
705 equatorial region (Morley, 2000), including southern Florida, parts of Central America, the
706 Caribbean, Brazil, west Africa, northern Australia, and SE Asia. However, evaporites have been
707 described from few of these, and mostly from islands in the Caribbean. The British Virgin Islands,
708 part of the Lesser Antilles, have an average annual rainfall of 1100 to 1200 mm, most of which is
709 delivered during the hurricane season. Hypersaline ponds, associated with mangrove forests, occur
710 along the coasts of the islands and those ponds with salinities above 175 ‰ during the dry season
711 precipitate gypsum (Jarecki & Walkey, 2006). In these ponds, the influx of seawater is through
712 seepage or marine flooding. In the Bahamas, gypsum precipitates in Big Pond on Eleuthra Island
713 (Glunk *et al*., 2011), whilst peats are accumulating on the coast of Florida nearby (Platt & Wright,
714 1992). Abundant gypsum is associated with lake and marsh clays of coastal lagoons in Belize

(Rejmankova *et al.,* 1996) and with thrombolites in Los Roques National Park, offshore Venezuela (Petrash *et al*., 2012). Gypsum crusts and microbial mats form in the hypersaline Gotomeer in the island of Bonaire, Netherlands Antilles (Kobluk & Crawford, 1990).

Highly saline wetlands are a feature of the Salum, Gambia and Casamance river estuaries of Senegal and The Gambia, in west Africa. These are caused by seasonally weak or absent freshwater flow in the rivers and extensive saline groundwater intrusion (Barusseau *et al*., 1985). Though pans constructed close to the rivers today produce salt, to the authors' knowledge, no natural evaporite deposits have been described from this region. A seasonal climate is also present in some parts of equatorial SE Asia where warm water carbonates are common today and in the Cenozoic in this marine gateway between the Pacific and Indian oceans (Wilson, 2012). However, evaporites are notably absent, possibly because of the high freshwater run-off from the surrounding landmasses and the lower sea salinity levels.

Some aspects of the sedimentology of the Ballagan Formation resemble those seen today in the Tigris–Euphrates delta (Aqrawi & Evans, 1994). However, the evidence cited above for a monsoonal regime in the region would seem to rule out the possibility that the Ballagan Formation floodplain represents a 'wetland within a dryland' environment with the common occurrence of salinas supplied by episodic influx of river water (Tooth & McCarthy, 2007; Pigati *et al.,* 2014). Wetlands in arid regions experience much lower rainfall than that determined for the Ballagan Formation by Kearsey *et al*. (2016).

Though coastal wetland evaporites are forming today in seasonal equatorial regions, there appear to be few examples described from the geological record. Gastaldo *et al*. (2006) suggested that the rarity of coastal marsh successions, for example, might be because of poor preservation potential. However, palustrine limestones are not rare: selected examples include from the Jurassic and Cenozoic of the UK (Andrews, 1986; Armenteros & Edwards, 2012), from the late Mississippian of Kentucky (Barnett *et al*., 2012) and from the upper Devonian in the Northwest Territories of

Canada (MacNeil & Jones, 2006). Gypsum is only a minor component in these successions. By contrast, from the Mid to Late Jurassic, evaporites formed seaward of coal swamps in Algeria, similar to the situation in the Bahamas and Florida today (Ziegler *et al*., 2003). The Lower Cretaceous, Leza Formation of the Cameros Basin, N Spain (Suarez-Gonzalez *et al.*, 2015) is an example of a coastal wetland succession with a diverse range of palaeoenvironments, like the Ballagan Formation, and including evaporitic lakes that deposited dolostone with gypsum. However, only the Canadian and Algerian examples were in equatorial locations at the time of deposition. The Ballagan Formation is therefore an unusual example in the geological record of a tropical, seasonal, coastal wetland that contains an abundance of evaporite forms and facies.

CONCLUSIONS

Small-scale evaporite deposits are a widespread and important facies of the coastal wetlands of equatorial Laurussia. They occur throughout the 13 million years spanned by the Tournaisian Ballagan Formation. The evaporites of Britain, Ireland and eastern Canada are apparently unique among widespread Tournaisian deposits in that they formed in an equatorial, strongly seasonal coastal wetland. There are few examples in the geological record and these Tournaisian deposits represent an unusual palaeoenvironment that is rarely preserved. Elsewhere, Tournaisian evaporites are associated with marginal marine to shallow marine carbonate systems.

In northern Britain, thin beds of laminated anhydrite, along with nodular gypsum and anhydrite (typically less than 1 to 2 m thick) occur locally throughout the Ballagan Formation in the Midland Valley, in the Tweed Basin and along the northern margin of the Northumberland – Solway basin. In this last example, anhydrite successions reaching >1000m characterize the depocentre indicating the importance and long-lived development of evaporites.

The evaporite deposits represent the existence of ephemeral brine pans to semi-permanent hypersaline lakes or salinas on the floodplain, though some also formed in the subsurface of widespread surrounding sabkhas. Monsoon storms may have initiated and recharged the lakes,

directly from precipitation and run-off, and importantly through the addition of marine waters during storm surges. These evaporites are compatible with a strongly seasonal climate for the region that has been proposed elsewhere from palaeosol types and geochemical proxies, and from palaeobotanical evidence. The thickness and extent of these Mississippian examples suggest that salinas and sabkhas were a significant component of this palaeoequatorial setting.

This research shows that the presence of small-scale evaporite deposits in the rock record do not necessarily imply an arid or semi-arid climate. The implications for our understanding of the palaeoenvironment and palaeoclimate in the Tournaisian are appreciated only alongside additional evidence from, for example, palaeosols. The widespread presence increases the diversity and complexity of habitats across large areas of the Tournaisian palaeoequatorial region in which the tetrapods first became terrestrialized.

ACKNOWLEDGEMENTS

This research formed part of the TW:eed Project (Tetrapod World: early evolution and diversification), led by Jenny Clack (University Museum of Zoology, Cambridge) and funded by N.E.R.C. consortium grants to the British Geological Survey (NEJ021067/1) and the Universities of Leicester (NE/J020729/1) and Southampton (NE/J021091/1). The Norham and Hoddom cores are archived in the National Geological Repository at BGS, Keyworth. The support of staff in curation and facilitating access is acknowledged. The paper is based on initial investigations of the evaporites from the Norham and Hoddom cores carried out by RC and FW as projects during their student studies at Leicester and Southampton respectively. We acknowledge gratefully Ian West's extensive support to FW (but to our dismay, he graciously declined to be a co-author). We thank Ian West, Noel Worley, Doug Holliday, Ian Somerville, Jim Hendry and an anonymous referee for comments that improved the manuscript. DM, TIK and MAEB publish with the permission of the Executive Director, British Geological Survey (N.E.R.C.).

REFERENCES

Aleali, M., Rahimpour-Bonab, H., Moussavi-Harami, R. and **Jahani, D.** (2013) Environment and sequence stratigraphic implications of anhydrite textures: a case from the Lower Triassic of the Central Persian Gulf. *J. Asian Earth Sci*., **75**, 110-125.

Alexeiev, D.V., Cook, H.E., Djenchuraeva, A.V. and **Mikolaichuk, A.V.** (2015) The stratigraphic, sedimentological and structural evolution of the southern margin of the Kazakhstan continent in the Tien Shan Range during the Devonian to Permian. In: *Geological Evolution of Central Asian Basins*

and the Western Tien Shan Range (Eds M.-F. Brunet, T. McCann and E. R. Sobel). *Geol. Soc. London, Spec. Publ.*, **427**, 231-269.

Alonso-Zarza, A.M. (2003) Palaeoenvironmental significance of palustrine carbonates and calcretes in the geological record. *Earth-Sci. Rev.*, **60**, 261-298.

Anderson, J.S., Smithson, T., Mansky, C.F., Meyer, T. and **Clack, J.** (2015) A diverse tetrapod fauna at the base of 'Romer's Gap'. PLoS ONE, **10**, 1-27.

Anderton, R. (1985) Sedimentology of the Dinantian of Foulden, Berwickshire, Scotland. *Trans. Roy. Soc. Edinb. Earth Sci.*, **76**, 7-12.

Andrews, J.E. (1986) Microfacies and geochemistry of Middle Jurassic algal limestones from Scotland. *Sedimentology*, **33**, 499-520.

Andrews, J.E. and **Nabi, G.** (1994) Lithostratigraphy of the Dinantian Inverclyde and Strathclyde Groups, Cockburnspath Outlier, East Lothian–North Berwickshire. *Scot. J. Geol.*, **30**, 105-119.

Andrews, J.E. and **Nabi, G.** (1998) Palaeoclimatic significance of calcretes in the Dinantian of the Cockburnspath Outlier (East Lothian-North Berwickshire). *Scot. J. Geol.,* **34**, 153-164.

Andrews, J.E., Turner, M.S., Nabi, G. and **Spiro, B.** (1991) The anatomy of an early Dinantian terraced floodplain: palaeo-environment and early diagenesis. *Sedimentology***, 38**, 271-287.

Aqrawi, A.A.M. and **Evans, G.** (1994) Sedimentation in the lakes and marshes (Ahwar) of the Tigris – Euphrates delta, southern Mesopotamia. *Sedimentology*, **41**, 755-776.

Armenteros, I. and **Edwards, N.** (2012) Palaeogeographic, palaeoclimatic, palaeohydrological and chemical/biochemical controls on accumulation of late Eocene coastal lacustrine-palustrine limestones, Southern England. *Sed. Geol.*, **281**. 101-118.

Armstrong, H.A. and **Purnell, M.A.** (1993) Thermal maturation of the Lower Carboniferous strata of the Northumberland Troup and Tweed Basin from conodont colour alteration index (DAI) data. *Proc. Yorks. Geol. Soc.*, **49**, 335-343.

Arthurton, R.S., Johnson, E.W. and **Mundy, D.J.C.** (1988) *Geology of the country around Settle*. Memoir, British Geological Survey, 1:50 000 geological sheet 60, England and Wales. London, HMSO, 147 pp.

Babel, M. (2004) Models for evaporite, selenite and gypsum microbialite deposition in ancient saline basins. *Acta Geol. Polonica*, **54**, 219-249.

Bahniuk, A., McKenzie, J.A., Perri, E., Bontognali, T.R.R., Vögeli, N., Rezende, C.E., Rangel, T.P. and **Vasconcelos, C.** (2015) Characterization of environmental conditions during microbial Mg-carbonate precipitation and early diagenetic dolomite crust formation: Brejo do Espinho, Rio de Janeiro, Brazil. In: *Microbial Carbonates in Space and Time: Implications for Global Exploration and Production* (Eds D.W.J. Bosence, K.A. Gibbons, D.P. Le Heron, W.A. Morgan, T. Pritchard and B.A. Vining). *Geol. Soc. London, Spec. Publ.*, **418**, 243-259.

Bailey, J.V., Orphan, V.J., Joye, S.B. and **Corsetti, F.A.** (2009) Chemotrophic microbial mats and their potential for preservation in the rock record. *Astrobiology*, **9**, 843-859.

Barbieri, R., Stivaletta, N., Marinangeli, L. and **Ori, G.G.** (2006) Microbial signatures in sabkha evaporite deposits of Chott el Gharsa (Tunisia) and their astrobiological implications. *Planet. and Space Sci*., **54**, 726-736.

Barnett, A.J., Wright, V.P. and **Crowley, S.F.** (2012) Recognition and significance of paludal dolomites: Lake Mississippian, Kentucky, USA. *Special Publication of the International Association of Sedimentologists,* **45**, 477-500.

Barusseau, J.P., Diop, E.H.S. and Saos, J.L. (1985) Evidence of dynamics reversal in tropical estuaries, geomorphological and sedimentological consequences (Salum and Casamance Rivers, Senegal). *Sedimentology*, **32**, 543-552.

Bateman, R.M. and **Scott, A.C.** (1990) A reappraisal of the Dinantian floras at Oxroad Bay, East Lothian, Scotland. 2. Volcanicity, palaeoenvironments and palaeoecology. *Trans. Roy. Soc. Edinb. Earth Sci*., **81**, 161-194.

Bennett, C.E., Howard, A.S., Davies, S.J., Kearsey, T.I., Millward, D., Brand, P.J., Browne, M.A.E., Reeves, E.J. and **Marshall, J.E.A.** (2017) Ichnofauna record cryptic marine incursions onto a coastal floodplain at a key early Mississippian tetrapod site. *Palaeogeogr., Palaeoclimatol., Palaeoecol.,* **468**, 287-300.

Bennett, C.E., Kearsey, T.I., Davies, S.J., Millward, D., Clack, J.A., Smithson, T.R. and **Marshall, J.E.A.** (2016) Early Mississippian sandy siltstones preserve rare vertebrate fossils in seasonal flooding episodes. *Sedimentology*, **63**, 1677-1700.

Bond, D.P.G. and **Wignall, P.B.** (2010) Pyrite framboids study of marine Permian-Triassic boundary sections: a complex anoxic event and its relationship to contemporary mass extinction. *Geol. Soc. Amer. Bull*., **122**, 1265-1279.

Bontognali, T.R.R., Vasconcelos, C., Warthmann, R.J., Bernasconi, S.M., Dupraz, C., Stromenger, C.J. and **McKenzie, J.A.** (2010) Dolomite formation within microbial mats in the coastal sabkha of Abu Dhabi (United Arab Emirates). *Sedimentology*, **57**, 824-844.

Browne, M.A.E. (1980) The Upper Devonian and Lower Carboniferous (Dinantian) of the Firth of Tay, Scotland. Institute of Geological Sciences Report Series 80/9.

Browne, M.A.E., Dean, M.T., Hall, I.H.S., McAdam, A.D., Monro, S.K. and **Chisholm, J.I.** (1999) A lithostratigraphical framework for the Carboniferous rocks of the Midland Valley of Scotland. British Geological Survey Research Report, RR/99/07.

Burgess, I.C. (1961) The fossil soils of the Upper Old Red Sandstone of South Ayrshire. *Trans. Geol. Soc. Glasgow,* **24,** 138-153.

Butler, G.P., Harris, P.M. and **Kendall, C.G.St.C.** (1982) Recent evaporites from the Abu Dhabi coastal flats. In: Deposition and Diagenetic Spectra of Evaporites (Eds C.R. Handford, R.G. Loucks and G.R. Davies), *SEPM Core Workshop* No. **3**, Calgary, 33-64.

Carney, J.N., Ambrose, K. and **Brandon, A.** (2001) Geology of the country between Loughborough, Burton and Derby. Sheet Description of the British Geological Survey, 1:50 000 Sheet 141 Loughborough (England and Wales), 92 pp.

Carter, D.C. and **Pickerill, R.K.** (1985) Algal swamp, marginal and shallow evaporitic lacustrine lithofacies from the Late Devonian – early Carboniferous Albert Formation, southeastern New Brunswick, Canada. *Atlantic Geology*, **21**, 69-86.

Cater, J.M.L., Briggs, D.E.G. and **Clarkson, E.N.K.** (1989) Shrimp-bearing sedimentary successions in the Lower Carboniferous (Dinantian) Cementstone and Oil Shale groups of northern Britain. *Trans. Roy. Soc. Edinb. Earth Sci.,* **80**, 5-15.

Chaboureau, A.-C., Donnadieu, Y., Sepulchre, P., Robin, C., Guillocheau, F. and **Rohais, S.** (2012) The Aptian evaporites of the South Atlantic: a climatic paradox? *Clim. Past*, **8**, 1047-1058.

Chagas, A.A.P., Webb, G.E., Burne, R.V. and **Southam, G.** 2016. Modern lacustrine microbialites: towards a synthesis of aqueous and carbonate geochemistry and mineralogy. *Earth-Sci Rev.*, **162**, 338-363.

Chisholm, J.I., McAdam, A.D. and **Brand, P.J.** (1989) Lithostratigraphical classification of Upper Devonian and Lower Carboniferous rocks in the Lothians. British Geological Survey, Technical Report WA/89/26.

Clack, J.A. (2002) An early tetrapod from 'Romer's Gap'. *Nature*, **418**, 72–76.

Clack, J.A., Bennett, C.E., Carpenter, D.K., Davies, S.J., Fraser, N.C., Kearsey, T.I., Marshall, J.E.A., Millward, D., Otoo, B.K.A., Reeves, E.J., Ross, A.J., Ruta, M., Smithson, K.Z., Smithson, T.R. and **Walsh, S.A.** (2016) Phylogenetic and environmental context of a Tournaisian tetrapod fauna. *Nature Ecology and Evolution,* **1**, 11 pp.

Clayton, G. (1986) Late Tournaisian miospores from the Ballycultra Formation at Cultra, County Down, Northern Ireland. *Irish J. Earth Sci.*, **8**, 73-79.

Clayton, G., Graham, J.R., Higgs, K., Sevastopulo, G.D. and **Welsh, A.** (1986) Late Devonian and early Carboniferous palaeogeography of southern Ireland and southwest Britain. *Annales de la Société géologique de Belgique*, **109**, 103-111.

Clayton, G. and **Higgs, K.** (1979) The Tournaisian marine transgression in Ireland. *J. Earth Sci., Roy. Dublin Soc*., **2**, 1-10.

Corfield, S.M., Gawthorpe, R.L., Gage, M., Fraser, A.J. and **Besly, B.M.** (1996) Inversion tectonics of the Variscan foreland of the British Isles. *J. Geol. Soc., London*, **153**, 17-32.

Costa, M., Telmer, K.H., Evans, T.L., Almeida, T.IR. and **Diakun, M.T.** (2015) The lakes of the Pantanal: inventory, distribution, geochemistry, and surrounding landscape. *Wetlands Ecol. Manage*., **23**, 19-39.

Coward, M.P. (1993) The effect of Late Caledonian and Variscan continental escape tectonics on basement structure, Paleozoic basin kinematics and subsequent Mesozoic basin development in NW Europe. *Geol. Soc. London Petrol. Geol. Conf.,* **4**, 1095-1108.

Davies, N. S. and **Gibling, M. R.** (2013) The sedimentary record of Carboniferous rivers: continuing influence of land plant evolution on alluvial processes and Palaeozoic ecosystems. *Earth-Sci Rev*., **120**, 40-79.

Day, J.B.W. (1970) *Geology of the country around Bewcastle*. Memoir, Geological Survey, Great Britain, England and Wales Sheet 12. 357 pp. HMSO.

Dean, M.T. (1997) Faunas from and biostratigraphy of the BGS Hoddom boreholes 1 and 2, Ecclefechan, Dumfriesshire. British Geological Survey Technical Report WH/97/115.

Domeier, M. and **Torsvik, T.H.** (2014) Plate tectonics in the late Paleozoic. *Geosci. Front.*, **5**(3), 303-350.

Dunham, K.C. (1973) A recent deep borehole near Eyam, Derbyshire. *Nature, Phys. Sci.*, **241**, 84-85.

Einsele, G. (2000) *Sedimentary Basins: Evolution, Facies and Sedimentary Budget*. 2nd edn. Springer, Belin-Heidelberg, 792 pp.

Eyles, V.A., Simpson, J.B. and **MacGregor A.G.** (1949) *Geology of Central Ayrshire*. Memoir, Geological Survey, Scotland (sheet 14). 2nd edn. HMSO, Edinburgh, 160 pp.

Falcon-Lang, H.J. (1999) The Early Carboniferous (Courceyan–Arundian) monsoonal climate of the British Isles: evidence from growth rings in fossil woods. *Geol. Mag.,* **136**, 177-187.

Falcon-Lang, H.J. (2004) Early Mississippian lycopsid forests in a delta-plain setting at Norton, near Sussex, New Brunswick, Canada. *J. Geol. Soc. London*, **161**, 969-981.

Francis, E.H., Forsyth, I.H., Read, W.A. and **Armstrong, M.** (1970) *The Geology of the Stirling district*. Memoir Geological Survey, Scotland (sheet 39). HMSO, Edinburgh.

Frantz, C.M., Petryshyn, V.A. and **Corsetti, F.A.** (2015) Grain trapping by filamentous cyanobacterial and algal mats: implications for stromatolite microfabrics through time. *Geobiology*, **13**, 409-423.

Gastaldo, R.A., Gibson, M.A. and **Blanton-Hooks, A.** (2006) A Late Mississippian back-barrier marsh ecosystem in the Black Warrior and Appalachian Basins. In: *Wetlands through Time* (Eds S.F. Greb and W.A. DiMichele), Geol. Soc. Am. Spec. Publ., **399**, 139–154.

Gawthorpe, R.L., Gutteridge, P. and **Leeder, M.R.** (1989) Late Devonian and Dinantian basin evolution in northern England and North Wales. In: *The Role of Tectonics in Devonian and Carboniferous Sedimentation in the British Isles* (Eds R.S. Arthurton, P. Gutteridge and S.C. Nolan), Occasional Publ. Yorks. Geol. Soc., **6**, 1-24.

Gibling, M.R., Culshaw, N., Rygel, M.C. and **Pascucci, V.** (2008) Chapter 6: The Maritimes Basin of Atlantic Canada: basin creation and destruction in the collisional zone of Pangea. In: *Sedimentary Basins of the World: The Sedimentary Basins of the United States and Canada* (Ed. A.D. Miall), **5**, 211-244.

Glunk, C., Dupraz, C., Braissant, O., Gallagher, K.L., Verrecchia, E.P. and **Visscher, P.T.** (2011) Microbially mediated carbonate precipitation in a hypersaline lake, Big Pond (Eleuthera, Bahamas). *Sedimentology*, **58**, 720-738.

Gregg, J.M., Bish, D.L., Kaczmarek, S.E. and **Machel, H.G.** (2015) Mineralogy, nucleation and growth of dolomite in the laboratory and sedimentary environment: a review. *Sedimentology*, **62**, 1749-1769.

Greig, D.C. (1988) *Geology of the Eyemouth district*. Memoir British Geological Survey, Scotland (sheet 34). HMSO, London, 78pp.

Griffith, A.E. and **Wilson, H.E.** (1982) *Geology of the country around Carrickfergus and Bangor*. Memoir Geological Survey Northern Ireland (sheet 29). HMSO, Belfast, 118 pp.

Gunatilaka, H.A. and **Shearman, D.J.** (1988) Gypsum-carbonate laminites in a recent sabkha, Kuwait. *Carbonates and Evaporites*, **3**, 67-73.

Gutteridge, P. (1987) Dinantian sedimentation and the basement structure of the Derbyshire Dome. *Geol. J.,* **22**, 25-41.

Hall, I.H.S., Browne, M.A.E. and **Forsyth, I.H.** (1998) *Geology of the Glasgow district.* Memoir Geological Survey, Scotland (sheet 30E). HMSO, London, 117 pp.

Hird, K. and **Tucker, M.E.** (1988) Contrasting diagenesis of two Carboniferous Oolites from South Wales: a tale of climatic influence. *Sedimentology*, **35**, 587-602.

Holliday, D.W. (1970) The petrology of secondary gypsum rocks: a review. *J. Sed. Petrol.,* **40**, 734-744.

Holliday, D.W. (1973) Early diagenesis in nodular anhydrite rocks. *Trans. Inst. Mining Metal*., **82**, B81-B84.

Holliday, D.W., Neves, R. and **Owens, B.** (1979) Stratigraphy and palynology of early Dinantian (Carboniferous) strata in shallow boreholes near Ravenstonedale, Cumbria. *Proc. Yorks. Geol. Soc*., **42**, 343-356.

Hovorka, S. (1992) Halite pseudomorphs after gypsum in bedded anhydrite – clue to gypsum-anhydrite relationships. *J. Sed. Petrol*., **62**, 1098-1111.

Irwin, H. (1980) Early diagenetic carbonate precipitation and pore fluid migration in the Kimmeridge Clay of Dorset, England. *Sedimentology*, **27**, 577-591.

Irwin, H., Curtis, C. and **Coleman, M.** (1977) Isotopic evidence for source of diagenetic carbonates formed during burial of organic-rich sediments. *Nature*, **269**, 209-213.

Jarecki, L. and **Walkey, M.** (2006) Variable hydrology and salinity of salt ponds in the British Virgin Islands. *Saline Systems*, **2**, 15 pp.

Kaiser, S.I., Aretz, M. and **Becker, R.T.** (2015) The global Hangenberg Crisis (Devonian–Carboniferous transition): review of a first-order mass extinction. In: Devonian Climate, Sea Level and Evolutionary Events (Eds R.T. Becker, P. Königshof and C.E. Brett), *Geol. Soc. London Spec. Publ.,* **423**, 423–429.

Kampschulte, A., Bruckschen, P. and **Strauss, H.** (2001) The sulphur isotope composition of trace sulphates in Carboniferous brachiopods: implications for coeval seawater, correlation with other geochemical cycles and isotope stratigraphy. *Chem. Geol*., **175**, 149-173.

Kasprzyk, A. and **Orti, F.** (1998) Palaeogeographic and burial controls on anhydrite genesis: the Badenian basin in the Carpathian Foredeep (southern Poland, western Ukraine). *Sedimentology*, **45**, 889-907.

Kearsey, T.I., Bennett, C.E., Millward, D., Davies, S.J., Gowing, C.J.B., Kemp, S.J., Leng, M.J., Marshall, J.E.A. and **Browne, M.A.E.** (2016) The terrestrial landscapes of tetrapod evolution in earliest Carboniferous seasonal wetlands of S.E. Scotland. *Palaeogeogr., Palaeoclimatol., Palaeoecol.,* **457**, 52-69.

Kendall, A.C. (1984) Evaporites. In: *Facies Models* (Ed. R.G. Walker), 2nd edn. Geol. Assoc. Can., pp. 259-296.

Kirkham, A. (1997) Shoreline evolution, aeolian deflation and anhydrite distribution of the Holocene, Abu Dhabi. *GeoArabia*, **2**, 403-416.

Kobluk, D.R. and **Crawford, D.R.** (1990) A modern hypersaline organic mud- and gypsum-dominated basin and associated microbialites. *Palaios*, **5**, 134-148.

Kreisa, R.D. and **Bambach, R.K.** (1973) Environments of deposition of the Price Formation (Lower Mississippian) in its type area, southwestern Virginia. *Am. J. Sci,* **273A**, 326-342.

Leeder, M.R. (1971) Initiation of the Northumberland Basin. *Geol. Mag.,* **108**, 511-516.

Leeder, M.R. (1974) Origin of the Northumberland Basin. *Scot. J. Geol.,* **10**, 283-296.

Leeder, M.R. (1975) Lower Border Group (Tournaisian) limestones from the Northumberland Basin. *Scot. J. Geol.,* **11**, 151-167.

Leeder, M.R. (1976) Palaeogeographic significance of pedogenic carbonates in the topmost Upper Old Red Sandstone of the Scottish Border Basin. *J. Geol.,* **11**, 21-28.

Leeder, M.R. and **Bridges P.H.** (1978) Upper Old Red Sandstone near Kirkbean, Dumfries and Galloway. *Scot. J. Geol.,* **14**, 267-272.

Leeder, M.R., Fairhead, D., Lee, A., Stuart, G., Clemmey, H., El Haddaheh, B. and **Green, C.** (1989) Sedimentary and tectonic evolution of the Northumberland Basin. In: *The Role of Tectonics in Devonian and Carboniferous sedimentation in the British Isles* (Eds R.S. Arthurton, P. Gutteridge and S.C. Nolan), Occasional Publ. Yorks. Geol. Soc., **6**, 207-223.

Llewellyn, P.G. and **Stabbins, R.** (1970). The Hathern Anhydrite Series, Lower Carboniferous, Leicestershire, England. *Trans. Inst. Mining Metal.*, **B79**, 1-15.

Lumsden, G.I., Tulloch, W., Howells, M.F. and **Davies, A.** (1967) *The geology of the neighbourhood of Langholm*. Memoir of the Geological Survey, Scotland (Sheet 11).

MacNeil, A.J. and **Jones, B.** (2006) Palustrine deposits on a late Devonian coastal plain – sedimentary attributes and implications for concepts of carbonate sequence stratigraphy. *J. Sed. Res*., **76**, 292-309.

Mastandrea, A., Perri, E., Russo, F., Spadafora, A. and **Tucker, M.** (2006) Microbial primary dolomite from a Norian carbonate platform, northern Calabria, southern Italy. *Sedimentology*, **53**, 465-480.

Matyja, H. (2008) Pomeranian basin (NW Poland) and its sedimentary evolution during Mississippian times. *Geol. J*., **43**, 123-150.

Miller, H. (1887) *The geology of the country around Otterburn and Elsdon*. Memoir Geological Survey, England and Wales (sheet 8). HMSO, London, 147pp.

Millward, D., Kearsey, T.I. and **Browne, M.A.E.** (2013) Norham West Mains Farm Borehole: operations report. British Geological Survey Internal Report, IR/13/033. 39 pp.

Mitchell, W.I. (1992) The origin of Upper Palaeozoic sedimentary basins in Northern Ireland and relationships with the Canadian Maritime provinces. In *Basins on the Atlantic Seaboard: Petroleum Geology, Sedimentology and Basin Evolution* (Ed. J. Parnell), *Geol. Soc. London Spec. Publ.,* **62**, 191-202.

Mitchell, W.I. (1997) Geological description of the area around Moneyneany (1:10 000 sheet 77NW Quadrant). Geological Survey of Northern Ireland Technical Report, GSNI/97/2.

Monro, S.K. (1999) *Geology of the Irvine district.* Memoir British Geological Survey, Scotland (sheet 22W and part of 21E). HMSO, London.

Morley, R.J. (2000) *Origin and Evolution of Tropical Rainforests*. Wiley, New York, 362 pp.

Murray, R.C. (1964) Origin and diagenesis of gypsum and anhydrite. *J. Sed. Petrol.,* **34**, 512-523.

Ogniben, L. (1957) Secondary gypsum of the sulphur series, Sicily, and the so-called integration. *J. Sed. Petrol.,* **27**, 64-79.

Owens, B., Gueinn, K.J. and **Cameron, I.B.** (1977) A Tournaisian miospore assemblage from the Altagoan Formation (Upper Calciferous Sandstone), Draperstown, Northern Ireland. *Pollen et Spores*, **19**, 313-324.

Paterson, I.B. and **Hall, I.H.S.** (1986) Lithostratigraphy of the late Devonian and early Carboniferous rocks in the Midland Valley of Scotland. British Geological Survey, Report, 18, No 3, 14pp.

Pattrick, R.A.D., Coleman, M.L. and **Russell M.J.** (1983) Sulphur isotopic investigation of vein lead-zinc mineralization at Tyndrum, Scotland. *Mineralium Deposita,* **18**, 477-485.

Petrash, D.A., Gingras, M.K., Lalonde, S.V., Orange, F., Pecoits, E. and **Konhauser, K.O.** (2012) Dynamic controls on accretion and lithification of modern gypsum-dominated thrombolites, Los Roques, Venezuela. *Sed. Geol*., **245-246**, 29-47.

Petty, D.M. (2010) Sequence stratigraphy and sequence boundary characteristics for upper Tournaisian (Mississippian) strata in the greater Williston basin area: an analysis of a third order cratonic carbonate-evaporite depositional cycle. *Bull. Canadian Petrol. Geol*., **58**, 375-402.

Philcox, M.E., Baily, H., Clayton, G. and **Sevastopulo, G.** (1992) Evolution of the Carboniferous Lough Allen Basin, Northwest Ireland. In: *Basins on the Atlantic seaboard: petroleum geology, sedimentology and basin evolution* (Ed. J. Parnell), *Geol. Soc. London Spec. Publ*., **62**, 203-215.

Pierre, C., Ortlieb, L. and **Person, A.** (1984) Supratidal evaporitic dolomite at Ojo de Liebre Lagoon: mineralogical and isotopic arguments for primary crystallization. *J. Sed. Petrol.,* **54**, 1049-1061.

Pigati, J.S., Rech, J.A., Quade, J. and **Bright, J.** (2014) Desert wetlands in the geological record. *Earth-Sci Rev.*, **132**, 67-81.

Platt, N.H. and **Wright, V.P.** (1992) Palustrine carbonates and the Florida Everglades: towards an exposure index for the freshwater environment. *J. Sed.Petrol*., **62**, 1058-1071.

Poty, E. (2016) The Dinantian (Mississippian) succession of southern Belgium and surrounding areas: stratigraphy improvement and inferred climate reconstruction. *Geologica Belgica*, **19**, 177-200.

Pracht, M. and **Somerville, I.D.** (2015) A revised Mississippian lithostratigraphy of County Galway (western Ireland) with an analysis of carbonate lithofacies, biostratigraphy, depositional environments and palaeogeographic reconstructions utilising new borehole data. *J. Palaeogeogr*., **4**, 1-26.

Read, W.A. and **Johnson, S.R.H.** (1967) The sedimentology of sandstone formations within the Upper Old Red Sandstone and lowest Calciferous Sandstone Measures west of Stirling, Scotland. *Scot. J. Geol.,* **3**, 242-267.

Rejmankova, E., Pope, K.O., Post, R. and **Maltby, E.** (1996) Herbaceous wetlands of the Yucatan Peninsula: communities at extreme ends of environmental gradients. *Int. Revue ges. Hydrobiol. Hydrogr.,* **81**, 223-252.

Retallack, G.J. and **Dilcher, D.L.** (1988) Reconstructions of selected seed ferns. *Ann. Miss. Bot. Gar*., **75**, 1010-1057.

Rose, W.C.C. and **Dunham, K.C.** (1977) *Geology and hematite deposits of South Cumbria*. Econ. Mem. Geol. Surv. G.B. England and Wales sheet 58 and part 48, 170 pp.

Rygel, M.C., Calder, J.H., Gibling, M.R., Gingras, M.K. and **Melrose, C.S.A.** (2006) Tournaisian forested wetlands in the Horton Group of Atlantic Canada. In: *Wetlands Through Time* (Eds S.F. Greb and W.A. DiMichele), *Geol. Soc. America, Special Paper*, **399**, 103–126.

Sánchez-Román, M., McKenzie, J.A., Rebello Wagener, A.deL., Rivadeneyra, M.A. and **Vasconcelos, C.** (2009) Presence of sulfate does not inhibit low-temperature dolomite precipitation. *Earth Planet Sci. Lett.,* **285**, 131-139.

Sanz-Montero, M.E., Rodríguez-Aranda, J.P. and **García del Cura, M.A.** (2009) Bioinduced precipitation of barite and celestite in dolomitic microbialites: examples from Miocene lacustrine sequences in the Madrid and Duero Basins, Spain. *Sed. Geol.*, **222**, 138-148.

Sanz-Rubio, E., Hoyos, M., Calvo, J.P. and **Rouchy, J.M.** (1999) Nodular anhydrite growth controlled by pedogenic structures in evaporite lake formations. *Sed. Geol.,* **125**, 195-203.

Schieber, J. (1999) Microbial mats in terrigenous clastics: the challenge of identification in the rock record. *Palaios*, **14**, 3-12.

Schieber, J. (2007) Microbial mats on muddy substrates – examples of possible sedimentary features and underlying processes. In: *Atlas of Microbial Mat Features Preserved within the Siliciclastic Rock Record.* (Eds J. Schieber, P.K. Bose, P.G. Eriksson, S. Banerjee, S. Sarker, W. Altermann and O. Catuneanu), pp. 117-133. Elsevier.

Schreiber, B.C. and **El Tabakh, M.** (2000) Deposition and early alteration of evaporites. *Sedimentology,* **47**, Suppl. 1, 215-238.

Scott, A.C. and **Meyer-Berthaud, B.** (1985) Plants from the Dinantian of Foulden, Berwickshire, Scotland. *Trans. Roy. Soc. Edinb.: Earth Sci.,* **76**, 13-20.

Scott, W.B. (1986) Nodular carbonates in the Lower Carboniferous, Cementstone Group of the Tweed Embayment, Berwickshire: evidence for a former sulphate evaporite facies. *Scot. J. Geol*., **22**, 325-345.

Shearman, D.J. (1966) Origin of marine evaporites by diagenesis. *Trans. Inst. Mining and Metallurgy*, **B75**, 208-215.

Shearman, D.J. (1978) Halite in sabkha environments. In: *Marine Evaporites* (Eds W.E. Dean and B.C. Schreiber), *SEPM Short Course*, **4**, 30-42.

Shearman, D.J. (1985) Syndepositional and late diagenetic alteration of primary gypsum to anhydrite. In: *Sixth International Symposium on Salt* (Eds B.C. Schreiber and L. Harmer), **1**, 41-50. Salt Institute, Alexandria, VA.

Shearman, D.J. and **Fuller, J.G.** (1969) Anhydrite diagenesis, calcitization and organic laminites, Winnipegosis Formation, Middle Devonian, Saskatchewan. *Bull. Canadian Petrol. Geol*., **17**, 496-525.

Sheridan, D.J.R., Hubbard, W.F. and **Oldroyd, R.W.** (1967) A note on Tournaisian strata in Northern Ireland. *Roy. Dublin Soc., Sci. Proc.,* Series A, **3**, 33-37.

Sibley, D.F. and **Gregg, J.M.** (1987) Classification of dolomite rock textures. *J. Sed. Petrol*., **57**, 967-975.

Smith, R.A. (1986) Permo-Triassic and Dinantian rocks of the Belfast harbour Borehole. British Geological Survey Report, **18**, No 6.

Smithson, T.R., Wood, S.P., Marshall, J.E.A. and **Clack, J.A.** (2012) Earliest Carboniferous tetrapod and arthropod faunas from Scotland populate Romer's Gap. *PNAS*, **109**, 4532-4537.

Stephenson, M.H., Williams, M., Monaghan, A.A., Arkley, S. and **Smith, R.A.** (2002) Biostratigraphy and palaeoenvironments of the Ballagan Formation (Lower Carboniferous) in Ayrshire. *Scot. J. Geol*., **38**, 93-111.

Stephenson, M.H., Williams, M., Leng, M.J. and **Monaghan, A.A.** (2004a) Aquatic plant microfossils of probable non-vascular origin from the Ballagan Formation (Lower Carboniferous), Midland Valley, Scotland. *Proc. Yorks. Geol. Soc*., **55**, 145-158.

Stephenson, M.H., Williams, M., Monaghan, A.A., Arkley, S., Smith, R.A., Dean, M., Browne, M.A.E. and **Leng, M.** (2004b) Palynomorph and ostracod biostratigraphy of the Ballagan Formation, Midland Valley of Scotland, and elucidation of intra-Dinantian unconformities. *Proc. Yorks. Geol. Soc*., **55**, 131-143.

Stott, D.F. and **Aitken, J.D.** (Eds) (1993) Sedimentary cover of the craton in Canada. *Geol. Surv. Canada, Geology of Canada*, 5, 825 pp.

Strank, A.R.E. (1985) The Dinantian biostratigraphy of a deep borehole near Eyam, Derbyshire. *Geol. J.*, **20**, 227-237.

Suarez-Gonzalez, P., Quijada, I.E., Benito, M.I. and **Mas, R.** (2015) Sedimentology of ancient coastal wetlands: insights from a Cretaceous multifaceted depositional system. *J. Sed. Res*., **85**, 95-117. DOI:10.2110/jsr.2015.07.

Taberner, C., Marshall, J.D., Hendry, J.P., Pierre, C. and **Thirlwall, M.F.** (2002) Celestite formation, bacterial sulphate reduction and carbonate cementation of Eocene reefs and basinal sediments (Igualada, NE Spain). *Sedimentology*, **49**, 171-190.

Tooth, S. and **McCarthy, T.S.** (2007) Wetlands in drylands: geomorphological and sedimentological characteristics, with emphasis on examples from southern Africa. *Prog. Phys. Geog.,* **31**, 3-41.

Van der Zwan, C.J., Boulter, M.C. and **Hubbard, R.N.L.B.** (1985) Climatic change during the lower Carboniferous in Euramerica, based on multivariate statistical analysis of palynological data. *Palaeogeogr., Palaeoclimatol., Palaeoecol.,* **52**, 1-20.

Vasconcelos, C. and **McKenzie, J.A.** (1997) Microbial mediation of modern dolomite precipitation and diagenesis under anoxic conditions (Lagoa Vermelha, Rio de Janeiro, Brazil). *J. Sed. Res.*, **67**, 378-390.

Ward, J. (1997) Early Dinantian evaporites of the Easton-1 well, Solway Basin, onshore, Cumbria, England. In: *Petroleum Geology of the Irish Sea and Adjacent Areas* (Eds N.S. Meadows, S.P. Trueblood, M. Hardman and G. Cowan). *Geol. Soc. London Spec. Publ.,* **124**, 277-296.

Warren, J.K. (2000) Dolomite: occurrence, evolution and economically important associations. *Earth-Sci Rev*., **52**, 1-81.

Warren, J.K. (2006) Evaporites: Sediments, Resources and Hydrocarbons. Springer-Verlag, Berlin-Heidelberg, 1035 pp.

Warren, J.K. (2010) Evaporites through time: tectonic, climatic and eustatic controls in marine and nonmarine deposits. *Earth-Sci. Rev*., **98**, 217-268.

Warren, J.K. and **Kendall, C.G.St.C.** (1985) Comparison of sequences formed in marine sabkha (subaerial) and salina (subaqueous) settings: modern and ancient. *Amer. Assoc. Petrol. Geol., Bull*., **69**, 1013-1023.

Waters, C.N., Somerville, I.D., Jones, N.S., Cleal, C.J., Collinson, J.D., Waters, R.A., Besly, B.M., Dean, M.T., Stephenson, M.H., Davies, J.R., Freshney, E.C., Jackson, D.I., Mitchell, W.I., Powell, J.H., Barclay, W.J., Browne, M.A.E., Leveridge, B.E., Long, S.L. and **McLean, D.** (Eds) (2011) *A revised correlation of Carboniferous rocks in the British Isles*. Geol. Soc. London Special Report, **26**, 186pp.

West, I.M. (1964) Evaporite diagenesis in the Lower Purbeck Beds of Dorset. *Proc. Yorks. Geol. Soc*., **34**, 315-330.

Wilkin, R.T., Barnes, H.L. and **Brantley, S.L.** (1996) The size distribution of framboidal pyrite in modern sediments: an indicator of redox conditions. *Geochim. Cosmochim. Acta*, **60**, 3897-3912.

Williams, M., Leng, M.J., Stephenson, M.H., Andrews, J.E., Wilkinson, I.P., Siveter, D.J., Horne, D.J. and **Vannier, J.M.C.** (2006) Evidence that Early Carboniferous ostracods colonised coastal flood plain brackish water environments. *Palaeogeogr., Palaeoclimatol., Palaeoecol.,* **230**, 299-318.

Williams, M., Stephenson, M.H., Wilkinson, I.P., Leng, M.J. and **Miller, C.G.** (2005) Early Carboniferous (Late Tournaisian-Early Viséan) ostracods from the Ballagan Formation, central Scotland, UK. *J. Micropal*., **24**, 77-94.

Wilson, M.E.J. (2012) Equatorial carbonates: an earth systems approach. *Sedimentology*, **59**, 1-31.

Witzke, B.J. (1990) Palaeoclimatic constraints for Palaeozoic palaeolatitutes of Laurentia and Euramerica. In: *Palaeozoic Palaeogeography and Biogeography* (Eds W.S. McKerrow and C.R. Scotese). *Geol. Soc. London, Memoir*, **12**, 57-73.

Wright, D.T. and **Wacey, D.** (2005) Precipitation of dolomite using sulphate-reducing bacteria from the Coorong Region, South Australia: significance and implications. *Sedimentology*, **52**, 987-1008.

Wright, V.P. (1982) Calcrete palaeosols from the lower Carboniferous Llanelly Formation, South Wales. *Sed. Geol*., **33**, 1-33.

Wright, V.P. (1990) Equatorial aridity and climatic oscillations during the early Carboniferous, southern Britain. *J. Geol. Soc. London*, **147**, 359-363.

Wright, V.P., Turner, M.S., Andrews, J.E. and **Spiro, B.** (1993) Morphology and significance of super-mature calcretes from the Upper Old Red Sandstone of Scotland. *J. Geol. Soc. London*, **150**, 871-883.

Young, G.M. and **Caldwell, W.G.E.** (2011) Early Carboniferous stratigraphy in the Firth of Clyde area: new information from the Isle of Bute. *Scot. J. Geol*., **47**, 143-156.

Young, G.M. and **Caldwell, W.G.E.** (2012) The Northeast Arran Trough, the Corrie conundrum and the Highland Boundary Fault in the Firth of Clyde, SW Scotland. *Geol. Mag*., **149**, 578-589.

Young, J.W. (1867) On the Ballagan Series of Rocks. *Trans. Geol. Soc. Glasgow*, **2**, 209-212.

Younger, P.L, Manning, D.A.C., Millward, D., Busby, J.P., Jones, C. R.C. and **Gluyas, J.G.** (2016) Geothermal exploration in the Fell Sandstone Formation (Mississippian) beneath the city centre of Newcastle upon Tyne, UK: the Newcastle Science Central Deep Geothermal Borehole. *Quart. J. Eng. Geol. Hydrogeol.,* **49**, 350-363.

Ziegler, A.M., Eshel, G., Rees, P.M., Rothfus, T.A., Rowley, D.B. and **Sunderlin, D.** (2003) Tracing the tropics across land and sea: Permian to present. *Lethaia*, **36**, 227-254.

Figures

Fig. 1. Distribution of Tournaisian and evaporite rocks in the Midland Valley of Scotland and Northumberland – Solway Basin. Key boreholes are shown; Com S2 – Cominco S2. Borehole metadata are given in Supplementary Data 1. Ballagan Formation outcrop from the British Geological Survey DiGMapGB © NERC 2015. Concealed evaporite subcrop in the Northumberland – Solway Basin after Ward (1997).

Fig. 2. Lower Mississippian stratigraphy in the Midland Valley of Scotland and Northumberland – Solway Basin (after Waters *et al*., 2011); KCBV – Kelso, Cottonshope and Birrenswark volcanic formations. Ballagan Formation (Browne, 1980) subsumes the Tyninghame Formation (Chisholm *et al*., 1989), Cementstone Group (Miller, 1887; Greig, 1988) and part of the Lower Border Group (Lumsden *et al*., 1967; Day, 1970; Leeder, 1974). The Kinnesswood, Ballagan and Clyde Sandstone formations comprise the Inverclyde Group (Browne *et al*., 1999). The palynostratigraphy of the Ballagan Formation is from Stephenson *et al*. (2002, 2004a, b), Williams *et al*. (2005) and Smithson *et al*. (2012).

Fig. 3. Distribution of evaporite occurrences in selected boreholes in the west and north of the Midland Valley of Scotland. The black curves within the stratigraphical columns represent the proportional thickness of grey, laminated siltstone/ mudstone per 10 m interval through the succession.

Fig. 4. Lithological logs and stratigraphical distribution of sedimentary characteristics of the Ballagan Formation in the Norham and Hoddom borehole cores. Main fluvial sandstone units in yellow. Note difference in scale between the logs.

Fig. 5. Photomicrographs of evaporite textures from the Norham West Mains Farm and Hoddom cores; A to F in crossed-polars. (A) Lozenge-shaped pseudomorphs of anhydrite after gypsum in very fine-grained sandstone cemented by anhydrite. Hoddom, depth 160.61 m. SSK70688. Field of view

2 mm. (B) Packed pseudomorphs of anhydrite after gypsum in dark dolomicrite matrix. Hoddom, depth 169.00 m. SSK70687. Field of view 3.3 mm. (C) Aphanitic cores and subparallel-aligned anhydrite in coalesced nodular mass within dolostone bed. Norham, depth 448.85 m. SSK38034. Field of view 2 mm. (D) Margin of nodular mass with interlayering of aphanitic anhydrite aggregates with host siltstone. Some of the anhydrite aggregates resemble gypsum crystal forms. Facies 2 at depth 467.90 m, Norham. SSK55670. Field of view 3.3 mm. (E) Aphanitic anhydrite in smaller nodules and around margin of larger mass, the centre of which is composed of granoblastic anhydrite (top). From Facies 2 at depth 493.54 m, Norham. SSK55673. Field of view 3.3 mm. (F) Granoblastic texture in anhydrite rock. Same unit as D, Norham depth 467.84 m. SSK55670. Field of view 3.3 mm.

Fig. 6. Sedimentary log illustrating the context of the evaporites in the saline – hypersaline lake facies association; Norham core, depth 445.84 to 451.58 m. A to F refer to photographs in Fig. 7.

Fig. 7. Core images for evaporite-bearing units in Fig. 6. (A) Facies 2b; (B and C) Facies 5; (D) Facies 1 (top and third from top) and Facies 5; (E) Facies 4; (F) Facies 5. All cores 102 mm across.

Fig. 8. Selected examples of evaporite facies from the Ballagan Formation. All except for C are from the Norham core, width of core and image 102 mm; C from the Hoddom core, width 46 mm; all depths are given below ground level. (A) Facies 1a, nodular anhydrite, depth 474.40 to 474.60 m; (B) Facies 1a, enterolithic vein, depth 468.05 to 468.16 m; (C) Facies 1b, beds of small nodules in fine-grained sandstone, depth 135.81 to 135.92 m. (D) Facies 3, pink nodular gypsum within dolomicrite matrix, cut by white gypsum veins; note thin unit of laminated dolomicrite beneath upper gypsum vein separating two nodule beds; depth 182.42to 182.85 m; (E) Anhydrite rock zone with stylolitic contact and traces of siltstone between nodules, Facies 2, 377.99 to 378.10 m; (F). Facies 5, ferroan dolostone containing anhydrite nodules; water escape structure at top of unit, depth 482.06 to 482.27 m. (G) Facies 4, alternating millimetric lamination in siltstone and anhydrite rock, depth 450.76 to 450.83 m;

1238 Fig. 9. Examples of Facies 2 from the Norham core (core width 102 mm). (A) Facies 2a, including
1239 separated nodular, anhydrite rock and protonodular zones. Note the water-escape structure at the
1240 top of the dolostone hosting the nodular zone. The protonodular zone is hosted in laminated
1241 siltstone and dolomitic siltstone. Depth 422.14 to 422.94 m. (B) Facies 2b, showing nodular and
1242 chicken-wire zones. At the top, the protonodular zone is weakly developed. Depth 436.98 to
1243 437.38 m. (C) Facies 2a (322.70 to 323.37 m) overlain by Facies 5 dolostone with evaporite nodules.
1244 Most of the evaporite mineral is secondary gypsum but the well defined nodular, anhydrite rock and
1245 protonodular zones are present in Facies 2. The protonodular zone at the base is hosted by
1246 laminated dolostone. Central section of core is polished to reveal textures.

1247 Fig. 10. Sedimentary features indicating the former presence of microbial mats in the Ballagan
1248 Formation. All depths given beneath ground level. (A) Protonodules of gypsum (gy) with rims of
1249 poikilotopic dolomite in interlaminated siltstone and very fine-grained sandstone at the base of
1250 Facies 2a. The dark laminae deformed by the protonodules are composed of planar-s to planar-e
1251 dolomite rhombs that are detailed in B. Largest protonodule is 6 mm across. Norham core, depth
1252 422.65 m. Scan of thin section SSK55656. Field of view 30 mm. (B) Electron backscatter image of
1253 detail of one of the dark dolomite laminae in A. Note thin films of clay minerals (c) associated with
1254 fine-grained pyrite (bright specks) and floating grains of quartz (q). Pore-fills of anhydrite (a) are also
1255 present. (C) Disrupted and torn strips of claystone (dark layers) interleaved with aphanitic anhydrite
1256 (pale areas). Facies 4, Norham, depth 450.70 m. Rectangle indicates location of D. Field of view
1257 26 mm across. Scan of thin section SSK70682. (D) Detail from right-hand side of C in plane-parallel
1258 light showing brownish clay-rich layers alternating with pale anhydrite dominated layers. The
1259 claystone laminae contain narrow strips of carbonaceous matter, scattered quartz and feldspar
1260 grains, pockets of anhydrite and randomly orientated mica plates. Field of view 2 mm. (E and F)
1261 Electron backscatter images of pyrite-rich (bright trails and specks) dolostone hosting protonodules
1262 of secondary gypsum (gy) with rims of planar-e dolomite (d). In E, the arrows indicate the margin of
1263 the gypsum nodule bed. Norham core, depth 182.42 m. SSK55666. (F) Detail of E showing the mesh-

like pyrite trails outlining the former presence of tubular structures interpreted as possible microbial filaments. Note the pyrite framboids (p) and entrapped grains of mica (m) and quartz (q).

Fig. 11. Secondary evaporite textures from the Norham West Mains Farm and Hoddom cores. A to F in crossed-polars. (A) Porphyrotopic gypsum (gy) with abundant anhydrite inclusions at margin of anhydrite (An) nodule. Matrix siltstone cut by gypsum vein. Norham, depth 421.54 m. SSK61191. Field of view 3.3 mm. (B) Gypsum (gy) nodules in dark dolomicrite (top right); rim to nodule of polymodal planar-e to planar-s dolomite. Norham, depth 182.61 m. SSK55666. Field of view 3.3 mm. (C) Porphyrotopic gypsum with anhydrite inclusions replaced by finer grained anhedral gypsum and overprinted by variable amounts of dolomite. Norham depth 377.71 m. SSK55651. Field of view 3.3 mm. (D) Gypsum nodules (gy) within laminated dolomicrite containing streaks of organic matter (c); granular gypsum vein to left. Norham depth 182.76 m. SSK55668. Field of view 3.3 mm. (E) Anhydrite vein, cutting anhydrite nodules (n) and silty dolostone (s); nodules heavily overprinted with polymodal planar-s dolomite. Norham depth 451.39 m. SSK61185. Field of view 3.3 mm. (F) Poikilotopic anhydrite cement in very fine-grained sandstone beneath dolomicrite with nodular anhydrite. Hoddom, depth 169.43 m. SSK42175. Field of view 1.5 mm.

Fig. 12. Cartoon to illustrate the evaporite palaeoenvironments.

Table 1. Summary of the petrographic characteristics of the evaporite forms in the Ballagan Formation.

Table 2. Summary of the diagenesis of the evaporite rocks in the Ballagan Formation. References cited support the interpretation except for 8 and 10 which are specific to these rocks.

Supplementary Data

1. Summary data for boreholes penetrating Tournaisian rocks in the UK.
2. Evaporite occurrences in the Norham cores.
3. Evaporite occurrences in the Hoddom cores.

Table 1. Summary of the petrographic characteristics of the evaporite forms in the Ballagan Formation.

Evaporite form	Description	Host rock and associated evaporite forms	Facies	Anhydrite texture	Gypsum textures	Dolomite texture
Pseudomorphs after halite	Disseminated euhedral and hopper crystals replaced in silt and sand	Siltstone and laminated fine-grained sandstone. Not associated with other facies	7	Not present	Not present	Not present
Pseudomorphs after primary gypsum	Euhedral and subhedral shapes to anhydrite aggregates up to 3 mm	Sandstone, dolostone and siltstone	4	Aphanitic aggregates	Not seen	Generally not overprinted
Protonodules	<5 mm diameter gypsum and anhydrite typically lying along lamination; also as dispersed, angular, irregular-shaped masses	Grey laminated siltstone, silty dolostone and dolostone; very thin dolomicrite laminae associated with protonodules	2	Aphanitic aggregates, some forms reminiscent of single gypsum crystals; inclusions in secondary gypsum protonodules	Porphyrotopic single or multiple crystals, some replacing several protonodules	Isolated crystals, rims and replacement of gypsum by polymodal planar-s rhombs with grain-size av. 0.11 mm, cloudy cores
Nodules gypsum	Round to angular nodules and coalesced masses; may form chicken-wire or enterolithic-like structures; some with diffuse margin.	Dolostone. Typically associated with many narrow and discontinuous late gypsum veins	3, 5	Inclusions abundant in gypsum; minor remnant areas aphanitic anhydrite	Porphyrotopic grains; small nodules may be single crystals; grain boundaries irregular, extinction undulose and contain anhydrite inclusions	Polymodal, planar-s rhombs at margin of nodule, with sporadic dispersed planar-e rhombs; with increasing dolomitization planar-s aggregates replace evaporite form.
Prismatic gypsum	Dispersed single and radiating aggregates originating from anhydrite nodule margin	Overprinting nodular or chicken-wire anhydrite	5	As for nodular anhydrite	Well terminated prismatic crystals up to 20 x 10 mm	None
Irregular nodules anhydrite and gypsum	Dispersed elongate aggregates with intricate, irregular margins	Dolostone; may pass down into thinly laminated evaporite - dolostone couplets	5	Aphanitic aggregates with some coarser elongate crystals	Porphyrotopic	Narrow margin polymodal planar-s rhombs, scattered unimodal planar-e to abundant close-packed aggregates of polymodal planar-s
Mosaic anhydrite	High proportion (up to 85%) of generally small (<1 cm) nodules dispersed through matrix.	Dolostone and siltstone. Typically grades into nodular or chicken-wire forms.	5	As for protonodular anhydrite	Not seen	Not seen
Nodules anhydrite	Round to elongate or angular and irregular nodules and nodular masses 1 to 15 cm across; margins sharp and smooth or cauliform; some narrow enclaves of siltstone or dolostone. Sinuous trains forming enterolithic veins	Common as isolated single and clustered masses in typically laminated siltstone and dolostone; lamination deformed above and below mass. Also occurs with chicken-wire and laminated anhydrite forms	1, 2, 5	Aphanitic, roughly circular to rhombohedral 'cores'; surrounded by parallel-aligned and sheaf-like aggregates of ragged laths, becoming decussate locally; patchily overgrown by stubby subhedral granular grains. Grains 0.0018 to 0.21 mm. Aligned texture typical at nodule margin	Nodules rimmed with porphyrotopic gypsum average 0.6mm; grain boundaries irregular, extinction undulose, and contain anhydrite inclusions	Margins rimmed with polymodal, planar-s; dispersed unimodal planar-e crystals within nodule to increasing overprint with polymodal planar-s aggregates; average grain size 0.1 mm.
Chicken-wire anhydrite	Mass of coalesced microcrystalline anhydrite nodules, separated by mm wide discontinuous relicts of siltstone or dolostone between nodules. Nodules are irregular and typically flattened, some elongated vertically.	Minor included siltstone or dolostone; associated with nodular and laminated forms.	2, 5	Aphanitic 'cores' and parallel-aligned, elongate crystals 0.0018 to 0.21 mm adjacent to nodule margin and in smaller nodules. Replaced in some samples by granoblastic anhydrite which increases from <0.1 mm near margin to 0.36 to 0.49 mm in centre.	Not seen	Not commonly present; sporadic dispersed unimodal, planar-s rhombs with cloudy cores and clear rims (av. 0.11 mm); sporadic dispersed unimodal planar-e rhombs.
Anhydrite-rock	Homogeneous microcrystalline anhydrite with lamination defined by discontinuous trails and enclaves of siltstone	Always in association with other facies. Sharp contacts with chicken-wire or nodular forms	2, 4	Nematoblastic to granoblastic; parallel aligned subsequent to elongate and equant anhedral crystals with average grain size 0.2mm	Replacement by veins of prismatic gypsum with abundant tiny anhydrite inclusions	Sporadic dispersed unimodal planar-s to planar-e rhombs, but when granoblastic texture fully developed dolomite is generally absent.
Laminated anhydrite	Mm-scale laminae with anhydrite	Interlaminated with siltstone or dolomicrite	4	Aphanitic anhydrite as lenticular and prismatic pseudomorphs after gypsum; or anhedral granular anhydrite	Not seen	Not seen
Veins anhydrite/ gypsum	Abundant narrow (<5mm), continuous or discontinuous, typically subhorizontal veins of gypsum or anhydrite; thicker veins of satin spar. Small, irregular	Veins cut all facies and are typically characteristic of exposed strata. Gypsum veins most abundant where gypsum is dominant evaporite form particularly with nodular gypsum. Anhydrite veins present in lower	1, 2, 3, 4, 5	Typically discontinuous fracture fills with anhedral granular (0.023 to 0.75 mm) anhydrite within siltstone and dolostone; also cutting nodular fibroradiate masses	1. Granular aggregates (average 0.4 mm) with anhydrite inclusions. 2. Stubby anhedral crystals without anhydrite inclusions. 3. Satin spar, coarse	Planar-s dolomite overgrowths to gypsum vein type 1

	discontinuous veins link evaporite masses	parts of boreholes associated with nodular anhydrite masses.		elongate laths, inclusion free, commonly grown from each side of vein.	
Cements	Gypsum or anhydrite (depth dependent)	Fine or very fine-grained sandstone; rarely dolostone and siltstone.	Poikilotopic crystals up to 1.5 mm	Poikilotopic crystals up to 1 mm.	Not seen

Table 2. Summary of the diagenesis of the evaporite rocks in the Ballagan Formation. References cited support the interpretation except for 8 and 10 which are specific to these rocks.

Phase	Mineralogy & texture	Where	Timing and depth	References
Primary gypsum	Former presence inferred from lenticular pseudomorphs of aphanitic anhydrite	Hoddom: in evaporite laminites and sandy siltstone beds Norham: sporadic at margin of nodules	Tournaisian; primary sediment and in shallow subjacent sediment	
Gypsum dehydration to anhydrite	Aphanitic anhydrite cores with wheatsheaf or fasciculate anhydrite surrounding; granoblastic anhydrite. Poikilotopic anhydrite cement	Aphanitic in Hoddom and Norham; granoblastic in Facies 2 Norham	Tournaisian; shallow subsurface	1, 7, 11
Bacterial fermentation diagenesis	Laminae of dolomite crystals 8 to 25 µm containing thin layers of clay minerals, corroded quartz grains and associated clumps of pyrite framboids	Putative microbial mats at base Facies 2 in Norham	Carboniferous, during burial 10 to 1000 m	6
Burial	Possible grain growth of granoblastic anhydrite, but otherwise little effect inferred; granular anhydrite veins	All	Carboniferous, to depths not exceeding *ca* 2.5 km	1, 2, 8
Rehydration - secondary gypsum	1. Porphyrotopic gypsum rims to evaporite nodules; anhydrite inclusions	Norham: 340 to 430 m	Late Carboniferous/ Early Permian exhumation. Differing depths in boreholes indicate different uplift histories related to their locations relative to the Southern Uplands	3, 5, 9
	2. Alabastrine secondary gypsum: replacement of nodules by anhedral gypsum with sutured margins and undulose extinction; abundant anhydrite inclusions	Norham: above 340 m: Hoddom above *ca* 153 m		
	3. Satin spar veins	Accompanies 2. Noted in all boreholes in Midland Valley and present in many surface exposures.		
Dolomitization	Medium-grained, polymodal planar-e to planar-s replacement rims to nodules, to planar-s replacement of nodules; cloudy cores, clear rims. Fe content increases with depth. Granoblastic anhydrite not affected.	Norham and Hoddom; non-planar seen below 450m in Norham, but not present in Hoddom	Late Carboniferous/ Early Permian or later. Non-planar dolomite suggests that temperature did not much exceed 60°C	12
Calcitization	Coarsely crystalline calcite and dolomite	Seen only at exposure, e.g. Burnmouth; also in Northern Ireland	Quaternary(?); near surface	4, 10

1 Aleali *et al*., 2013; 2 Armstrong & Purnell, 1993; 3 Corfield *et al*., 1996; 4 Griffith & Wilson, 1982; 5 Holliday, 1970; 6 Irwin, 1980; 7 Kasprzyk & Orti, 1998; 8 Kearsey *et al*., 2016; 9 Ogniben, 1957; 10 Scott, 1986; 11 Shearman & Fuller, 1969; 12 Warren, 2000

APPENDIX 1

BORE NAME	BGS Registered Number	Easting	Northing	Total depth metres	Tournaisian thickness metres	Formation	Formation beneath	Formation above	Date drilled	No evaporite units
Argyle Brewery, Edinburgh	NT27SE/70	325776	673432	224	>128.40	Ballagan	Kinnesswood?	Not seen	1912	15
Ascog	NS06SE/8	209865	663020	252.72	33.09	Ballagan	Kinnesswood	Clyde Sandstone	1978	0
Barnhill	NS47NW/2	242690	675710	288.98	123.08	Ballagan	Kinnesswood	Clyde Sandstone	1977	30
Belfast Harbour No 1	29/885	147550	533680	522.81	>199.49	Ballycultra	Not seen	Coolbeg Basal Breccia	1978	
Birnieknowes	NT77SE/9	375798	673168	508.2	200.21	Ballagan	Kinnesswood	Gullane	1968	0
Blairmulloch	NS52NE/21	256050	628200	212.98	>166.58	Ballagan	Not seen	Clyde Sandstone	1996	34
Burnside	NS73SE/52	278615	633717	211.93	>35.43	Ballagan	Not seen	Clyde Sandstone	1980	0
Butlins, Ayr	NS31NW/2	230550	618460	90.85	>59.60	Ballagan	Kinnesswood	Not seen	1963	0
Cominco S2	SD86SW/6	384910	463450	426.35	>38.5	Stockdale Farm	Bot seen	Faulted	1968	?
Dalfram No 1	NS62NE/2	266330	626710	80.64	>45.00	Ballagan	Not seen	Clyde Plateau Volcanic	1926	0
Dalfram No 2	NS62NE/1	265967	626502	49.12	>25.80	Ballagan	Not seen	Not seen	1926	0
Deaconhill	NS43SE/81	248927	631526	196.64	150.03	Ballagan	Kinnesswood	Lower Limestone	1981	12
East Doura	NS43SW/76	244980	631220	157.28	>83.40	Ballagan	Not seen	Clyde Plateau Volcanic?	1912	0
East Dron	NO11NW/24	313600	715720	244.08	>209.54	Ballagan	Kinnesswood	Not seen	1971	114
East Linton 2	NT57NE/2	359664	677091	488.6	>418.17	Ballagan	Not seen	Garleton Hills Volcanic	1970	0
Easton 1	NY47SW/15	344124	571694	2609.09	>1197.87	Lyne	Not seen	Fell Sandstone	1990	120
Everton	NS27SW/5	221450	671035	50.69	>50.69	Ballagan	Kinnesswood	Not seen	1977	1
Eyam	SK 27 NW 15	420960	376030	1851.05	73.61	Middleton Dale Anhydrite	Lower Palaeozoic	Woo Dale	1971	
Glenrothes	NO20SE/385	325617	703144	567.65	157.43	Ballagan	Kinnesswood	Pathhead	1986	47
Harelaw	NS43SW/98	241660	633000	69.76	>9.17	Ballagan	Not seen	Kirkwood	1976	0
Harpertoun, Kelso	NT73NW/3	374761	639161	119	>53.14	Ballagan	Faulted	Not seen	1950	3
Hathern No 1	SK52SW 3	451580	324160	634.59	>97.23	Hathern Anhydrite	Not seen		1954	
Hoddom No 2	NY17SE/3	316410	572850	199.74	>59.90	Ballagan	Not seen	Lyne	1994	128
Hutton Castle Barns	NT85SE/1	389130	654110	183.19	>142.44	Ballagan	Kinnesswood	Not seen	1927	11
Inch of Ferryton	NS99SW/333	290777	690150	2441	48.80	Ballagan	Stratheden Group	Strathclyde Group	1986	0
Kipperoch	NS37NE/20	237270	677420	300.57	>49.70	Ballagan	Kinnesswood	Not seen	1977	0
Knocknairshill	NS37SW/10	230560	674380	294.96	70.87	Ballagan	Kinnesswood	Clyde Sandstone	1978	17
Leven Seat Well	NS95NE/146	296577	657795	1524	>192.02	Ballagan	Not seen	Volcanic rocks	1988	0
Little Freuchie No 2	NO20NE/16	327510	706450	59.43	>54.40	Ballagan	Not seen	Not seen	1979	0
Loch Humphrey	NS47NE/1	245820	675550	423.48	>162.95	Ballagan	Not seen	Clyde Sandstone	1978	64
Long Eaton No 1	SK43SE 161	446400	331660	2752.34		Hathern Anhydrite			1988	
Longhorsely	NZ19SW/6	414442	592553	1828.8	>196.6	Lyne	Not seen	Fell Sandstone	1986	0
Mains of Errol	NO22SW/29	323800	721900	97.87	>24.99	Ballagan	Kinnesswood	Not seen	1971	5
Marshall Meadows	NT95NE/5	397973	656858	313.23	>107.77	Ballagan	Not seen	Fell Sandstone	1970	0
Middlemass, Kelso	NT73SW/10	372638	634020	101	>86.10	Ballagan	Kinnesswood	Not seen	1952	16
Newburgh old	NO21NW/4			173.4	>126.37	Ballagan	Not seen	Not seen	1920	0
Newburgh B	NO21NW/7	323200	718520	60.39	>30.39	Ballagan	Not seen	Not seen	1971	2
Norham West Mains Farm	NT94NW/20	391600	648130	501.33	>497.10	Ballagan	Not seen	Not seen	2013	50
Scottish Parliament Well	NT27SE/449	326700	673800	100.5	>78.70	Ballagan	Not seen	Not seen	1999	0
Spilmersford	NT46NE/73	345694	669019	918.92	>258.24	Ballagan	Fault	Intrusion	1967	0
Stirling No 1 (Kaimes)	NS79SE/21	277200	694540	132.28	>28.30	Ballagan	Not seen	Clyde Sandstone	1961	0
Tak-ma-Doon	NS78SW/5	272910	680530	85.64	19.65	Ballagan	Kinnesswood	Clyde Plateau Volcanic	1978	0
West Dron	NO11NW/25	313480	716140	44.26	>40.94	Ballagan	Not seen	Not seen	1972	2
Westfield 3038	NT29NW/486	320896	699342	164.92	73.12	Ballagan	Not seen	Not seen	1972	0

Norham West mains Farm Borehole				Evaporite occurrences							
Unit no	Top	Base	Thickness	Evaporite description	Evaporite facies	Containing unit	Unit above	Unit below	Core photo no	Dave sheet no	Notes
1	28.75	28.88	0.13	dispersed small crystals gypsum in disrupted laminated cementstone; ?gypsum residue bed	6	laminated cementstone	laminated siltstone + very fine grained sandstone	laminated siltstone + very fine grained sandstone	5		within cementstone-laminated siltstone succession
2	36.22	36.26	0.04	lenticular carbonate-rich area, possibly residue bed after gypsum	6	laminated, brecciated cementstone with carbonate-rich masses	laminated grey siltstone	cross-bedded sandstone	6		siltstone-carbonate-evaporite unit within fluvial sandstone succession; ?residue bed
3	50.13	50.17	0.04	spongy fine-grained calcite fragments; rather rotted	6	laminated grey siltstone	cementstone	sandy siltstone	9		siltstone-carbonate-evaporite unit within fluvial sandstone succession; ?residue bed
4	63.56	63.59	0.03	gypsum nodules/veins 2cm x width of core; core broken, not true depth	1	grey siltstone	grey siltstone, carbonate rich, + cementstone	grey siltstone, carbonate rich, + cementstone	12		various laminated siltstone-cementstone successions separated by thin beds of sandy siltstone
5	66.77	67.13	0.36	in upper part areas up to 4mm across ?gypsum	5	cementstone	laminated grey siltstone	sandy siltstone	12		
6	67.22	67.56	0.34	gypsum nodules; irregular elongate masses along lamination; laminae deformed around nodules; horizontal gypsum vein at top	1	laminated grey siltstone	microconglomerate; 8cm thick; brecciated top (=surface)	laminated siltstone + very fine grained sandstone	13		
7	68.10	68.25	0.15	sporadic gypsum nodules; palaeosol surface 5cm above nodules	1	laminated very fine grained sandstone	rooted top to inseptisol or gleysol, overlain by microconglomerate	laminated very fine grained sandstone	13		
8	182.42	182.96	0.54	beds close-packed nodules gypsum; subordinate dolostone matrix	3	dolomite mudstone interstices	laminated grey siltstone, sporadic gypsum crystals; base x-bedded sandstone 18cm above	laminated grey siltstone	36	1	succession 182.21-185.35m laminated grey siltstone-cementstones; evaporite bed near top; extensive burrowing lower part; palaeosol below, x-bedded sandstone above
9	190.25	190.35	0.10	small gypsum nodules along laminae; contorted	1	laminated grey dolomitic siltstone	grey siltstone	grey siltstone	38		cementstone-laminated siltstone succession
10	222.35	222.47	0.12	protonodular gypsum	5	bioturbated laminated cementstone	cementstone	cementstone	45		cementstone-laminated siltstone succession
11	229.21	229.43	0.22	small gypsum nodules	1	bioturbated sandsone	cementstone	organic rich siltstone	46		cementstone-laminated siltstone succession
12	232.73	232.78	0.05	coalesced nodular gypsum nodules	5	dolomite mudstone	laminated grey siltstone	bioturbated grey siltstone	47	2	cementstone-laminated siltstone succession
13	239.56	239.61	0.05	siltstone nodule with sporadic gypsum crystals	5	cementstone	cementstone	microconglomerate	48		cementstone-laminated siltstone succession
14	276.77	276.92	0.15	vug-like areas up to 2mm filled with fanned aggregates of gypsum at base	5	cementstone, biotaurbated base, homogeneous centre, brecciated top	siltstone	laminated siltstone	56		cementstone-laminated siltstone succession
15	300.51	300.64	0.13	Irregular nodular masses gypsum with anhydrite centres, very undulose top and base with deformation of lamination; thickness 5-13cm	5	dolomite mudstone	laminated grey siltstone; laminae deformed by evaporite bed; base of laminated sandstone 42cm above	laminated grey siltstone; laminae deformed by evaporite bed	61	3	cementstone-laminated siltstone succession
16	322.35	322.70	0.35	diffuse and/or irregular micronodular aggregates anhydrite; pervasive subhorizontal gypsum veins	5	dolostone with thin intercalated grey siltstone laminae	intensely bioturbated grey siltstone	dolostone with anhydrite	66	4	
17	322.75	323.37	0.62	Complex evaporite succession: chickenwire anhydrite on laminated anhydrite; protonudular anhydrite along laminae at base	2a	laminated dolostone with thin intercalations grey silt	dolostone with anhydrite	laminated grey siltstone	66	4	succession grey siltstone-cementstone 320.40-325.55m (5.15m); evaporites in centre; beneath and above extensive burrowing Asterozoa, Chondrites/Phycosiphon near top; base on rooted
18	323.52	323.83	0.31	diffuse and/or irregular micronodular aggregates anhydrite; ?laminated top with vertical anhydrite xstls; pervasive subhorizontal gypsum veins	5	dolostone	laminated grey siltstone	laminated grey siltstone	66	5	layer; upper contact coarsening upward units of f sandstones ripple-laminated.
19	330.33	330.39	0.06	microcrystalline coalesced nodular mass anhydrite + some gypsum ?enterolithic vein	1	grey dolostone	grey siltstone	grey siltstone	67	6	
20	330.47	330.66	0.19	nodular masses gypsum aggregates; subhorizontal gypsum veins	5	laminated siltstone; deformed and some in dolostone below	dolostone	grey siltstone	67	6	succession 329.09-332.66m (3.57m) grey laminated siltstone, bioturbated organic rich at top; base rooted palaeosol; overlain by ripple-laminated sandstone
21	330.69	330.88	0.19	nodular masses gypsum aggregates; subhorizontal gypsum veins	5	dolostone	grey siltstone	dolostone, bioturbated silty top	67	6	
22	342.93	343.18	0.25	elongate nodular masses anhydrite fringed with gypsum; secondary gypsum nodules; dolostone nodule connecting secondary gypsum veins	1	grey siltstone, dolostone nodule; deformed laminae	grey siltstone, weakly laminated; cementstone top at 342.29 is cracked or base of microconglomerate at 342.10	bioturbated very fine grained sandstone + siltstone	70		cementstone-laminated siltstone succession
23	377.61	378.25	0.64	Complex unit: nodular masses anhydrite, gypsum at top, on chickenwire anhydrite, on laminated anhydrite	2a	siltstone matrix in chickenwire part	laminated siltstone overlain by complex cementstone with bioturbated top and overlain by sandstone with climbing ripples	laminated and bioturbated siltstone + very fine grained sandstone	77	7	laminated siltstone-cementstone succession; sandy siltstone below; fgr sandstone with climbing ripple lamination above. Possible erosion surface at top of evaporite unit.
24	421.10	421.33	0.23	nodular masses anhydrite with fringing gypsum; secondary pink gypsum veins	1	grey siltstone; deformed lamination	laminated grey siltstone	cementstone with evaporite	86	8	
25	421.33	421.70	0.37	complex unit: nodular masses anhydrite in dolostone, cumulose margin to nodules on laminated anhydrite; lamination at angle to sediment below; gypsum protonodules below	2a	dolostone on grey siltstone	grey siltstone	laminated dolomitised siltstone	86, 87	8	
26	422.14	422.94	0.80	Complex unit: coalesced nodular masses anhydrite on laminated anhydrite with fringing pink gypsum; anhydrite protonodules along lamination below	2a	dolostone on laminated black siltstone	laminated black siltstone with dolomite cement	cross-laminated dolomite cemented siltstone	87	9	succession 418.73-423.53m (4.80m), laminated siltstone - cementstones, with some ripple laminated and burrowed fgr sandstone at top; evaporite beds in lower half; underlain by v thin conglomerate beds (lowest entry is below these); overlain by basal
27	423.40	423.57	0.17	protonodular anhydrite along lamination	1	dolomite-cemented grey siltstone	laminated grey siltstone	homogeneous cementstone	87	10	conglomerate of cross-bedded sandstone
28	423.69	423.81	0.12	nodular anhydrite/gypsum mass	5	dolostone	homogeneous cementstone	grey siltstone	87	10	
29	424.09	424.17	0.08	streaky irregular masses anhydrite with fringing gypsum; secondary gypsum veins	5	dolostone, laminated, deformed around nodules	dolostone	laminated dolostone	87	10	
30	435.75	436.08	0.33	irregular nodular masses gypsum up to 7cm across; later fracture fills of gypsum	1	grey siltstone	cementstone	laminated grey siltstone	89, 90		
31	436.98	437.38	0.40	protonodular gypsum along laminae in siltstone; on laminated anhydrite with contorted siltstone enclaves; on nodular masses anhydrite/gypsum in dolostone matrix	2b	grey siltstone at top on cementstone	laminated siltstone	intensely bioturbated dolomite cemented grey siltstone	90	11	succession 435.04-439.10m (4.06m) dolomite-cemented siltstone-cementstone-laminated siltstone; uppermost part bioturbated vfgr sandstone; Naiadites + Modiolus in siltstone; underlain by pedogenically altered siltstone; overlain by cross-bedded sandstone.
32	446.10	446.71	0.61	protonodular gypsum along laminae in siltstone; on nodular masses gypsum/anhydrite in dolostone; on laminated anhydrite with siltstone enclaves; on nodular masses microcrystalline anhydrite in siltstone matrix	2b	grey laminated siltstone and cementstone	homogeneous cementstone; relict laminae	bioturbated cementstone + grey siltstone	92	12	
33	447.98	448.57	0.59	nodular masses anhydrite at top of cementstone, irregular bulbous contacts base, undulating sharp top; isolated nodules small below	5	bioturbated, contorted laminae dolomitised siltstone/sandstone	laminated grey siltstone with very fine grained sandstone lenses	laminated siltstone	92	13	
34	448.81	448.89	0.08	nodular masses anhydrite	1	grey siltstone	laminated grey siltstone with sandstone lenses; sporadic protonodules	grey siltstone	92	14	Laminated siltstone- cementstone succession 445.84-451.58m (5.74m); microconglomerate below, overlain by ripple-laminated vfgr sst. Siltstone extensively bioturbated in upper part. Cmst of Facies 1a,2, 3b, 5
35	449.13	449.31	0.18	nodular masses gypsum; secondary gypsum veinlets	1	grey siltstone; disrupted lamination	laminated grey siltstone with sandstone lenses	laminated black siltstone	92	14	
36	449.37	449.63	0.26	bulbous masses gypsum at top middle and base in both cmst + siltstone	5	complex cementstone unit, intercalations grey siltstone	laminated black siltstone; soft sediment deformed	cementstone, silty-type with remnant lamination	92	14	
37	450.50	451.14	0.64	Complex unit of nodular and laminated anhydrite, in part contorted	4	grey laminated siltstone and cementstone	laminated grey siltstone; interlaminated very fine grained sandstone	laminated cementstone	93	15	
38	451.25	451.42	0.17	downward increasing abundance of irregular small nodular masses of microcrystalline anhydrite; anhydrite protonodules in lowest part along lamination	5	cementstone	laminated dolostone	laminated grey micritic cementstone, mud-rich	93	15	
39	466.16	466.47	0.31	microcrystalline nodular masses anhydrite; minor protonodules at top and base	2b?	laminated black silt	laminated dolostone	grey siltstone	96	16	
40	467.69	468.16	0.47	Complex unit of nodular, chicken-wire and laminated anhydrite; nodular masses at base ?enterolithic vein	2b	laminated black siltstone and dolostone	laminated grey siltstone	laminated grey siltstone	96	17	Laminated siltstone- cementstone succession 470.75-465.64m (5.11m); microconglomerate below, overlain by ripple-laminated vfgr sst. Siltstone extensively bioturbated in part; Modiolus + Naiadites
41	469.50	469.56	0.06	nodular mass anhydrite with cementstone enclaves; irregular base, smooth undulating top	5	laminated muddy cementstone	cementstone	siltstone with carbonate laminae	97		
42	469.77	470.03	0.26	small gypsum crystals	5	laminated cementstone	cementstone	laminated siltstone	97		
43	474.40	474.60	0.20	nodular masses anhydrite; protonodular anhydrite at base	1	cementstone, silt-rich	cementstone	cementstone	98	18	cementstone-laminated siltstone succession
44	482.08	482.25	0.17	coalesced nodules anhydrite in dolomite matrix	5	cementstone; tepee structure at top	laminated grey siltstone with ostracods, bivalves	laminated grey siltstone with ostracods, bivalves	99	19	cementstone-laminated siltstone succession
45	482.29	482.62	0.33	nodular and chicken-wire masses up to 8cm pink gypsum	5	grey siltstone; lamination faint	laminated grey siltstone with ostracods, bivalves	structureless grey siltstone	99	19	
46	484.01	484.63	0.62	irregular chicken-wire masses; very irregular outline zig-zag pattern	5	cementstone	microconglomerate	laminated grey siltstone; trails protonodular gypsum? along lamination	100		cementstone-laminated siltstone succession
47	487.70	488.15	0.45	nodules gypsum/calcite	1	in lower part of red siltstone palaeosol	cementstone	grey, laminated siltstone	100		
48	493.05	494.09	1.04	complex unit with nodular anhydrite; chickenwire anhydrite; laminated anhydrite; isolated nodules and protonodules below	2a	laminated dolostone and dolomite cemented siltstone	laminated limestone	laminated siltstone	101, 102	20	cementstone-laminated siltstone succession topped by pedogenicly altered sandy siltstone; ripple-laminated sandstone below
49	498.56	498.58	0.02	elongate nodular	5	reddened dolostone	dolostone	laminated siltstone	103	21	
50	499.02	499.29	0.27	microcrystalline anhydrite masses; very irregular margins with disruption of laminae, some disseminated fine anhydrite along lamination	1	laminated siltstone	dolostone	palaeosol, siltstone	103	21	cementstone-laminated siltstone succession; sandy siltstone bedlow; ripple laminated sandstone above

Unit no	Top	Base	Thickness	Evaporite description	Evaporite facies	Containing unit	Unit above	Unit below
1	131.49	132.17	0.68	decreasing protonodules % anhydrite/gypsum upwards		bedded siltstone	siltstone	siltstone
2	132.82	133.64	0.82	gypsum protonodules		bedded siltstone	siltstone	dolostone
3	133.64	134.22	0.58	anhydrite nodules with gypsum overgrowths	5	dolostone	bedded siltstone	mgr sandstone
4	135.81	135.92	0.11	2 beds protonodules anhydrite, c 20mm; upper unit nodules concentrated at top		fine grained sandstone	siltstone, thin interbeds vfgr sandstone	sandy siltstone
5	136.18	136.30	0.12	nodules anhydrite with gypsum overgrowths; decrese upwards	5	dolostone	sandy siltstone	laminated siltstone with vfgrsandstone interbeds
6	136.30	136.94	0.64	bedded gypsum/anhydrite		siltstone and fine grained sandstone	dolostone	siltstone
7	136.94	137.08	0.14	anhydrite bands in centre		siltstone	siltstone and fine grained sandstone	sandstone
8	137.08	138.56	1.48	anhydrite layers 0.07 at 137.62 and 138.19		very fine to finegr sandstone	siltstone	anhydrite bed
9	138.56	138.62	0.06	anhydrite with prismatic gypsum overprint		siltstone	sandstone	vfgr sandstone
10	138.88	138.99	0.11	anhydrite with prismatic gypsum overprint	5	dolostone	sandstone	sandstone
11	139.13	139.21	0.08	bands small protonodules		very fine gr sandstone	sandstone	dolostone
12	139.21	139.35	0.14	packed zones small nodules anhydrite, becoming chickenwire in lower part		very fine gr sandstone	sandstone	siltstone
13	139.35	139.48	0.13	anhydrite with prismatic gypsum overprint	5	dolostone	siltstone	laminated sandstone
14	139.48	139.68	0.20	anhydrite nodules with prismatic gypsum overgrowths	5	dolostone	dolostone	dolostone
15	141.24	141.32	0.08	anhydrite nodules + prismatic gypsum		siltstone	siltstone	dolomite cemented sandstone
16	141.32	141.54	0.22	layers of anhydrite protonodules		dolomite cemented sandstone	siltstone with evaporite	siltstone
17	141.54	141.94	0.40	anhydrite nodules, decreasing upward		siltstone	siltstone	dolostone
18	141.94	142.05	0.11	small anhydrite nodules	5	dolostone	siltstone	siltstone
19	142.05	142.32	0.27	upward increasing nodule %		siltstone	dolostone	dolostone
20	142.32	142.53	0.21	anhydrite nodules	5	dolostone	siltstone	siltstone
21	142.53	142.60	0.07	anhydrite nodule		siltstone	dolostone	dolostone
22	142.60	142.80	0.20	anhydrite nodules	5	dolostone	siltstone	siltstone
23	142.80	142.85	0.05	anhydrite nodules		siltstone	dolostone	vfgr sandstone
24	142.85	144.78	1.93	sporadic anhydrite nodules; prismatic gypsum overprint at top	5	dolomite cemented very fgr sandstone, locally bioturbated	siltstone	silty, vfgr sandstone, laminated
25	144.78	144.86	0.08	anhydrite protonodules		silty, vfgr sandstone, laminated	dolomite cemented very fgr sandstone, locally bioturbated	dolostone
26	144.86	145.20	0.34	gypsum protonodules	5	dolostone	silty, vfgr sandstone, laminated	siltstone, laminated
27	145.23	145.44	0.21	some anhydrite nodules, % decreasing upward		dolomite cemented vfgr sandstone	siltstone	bedded vfgr sandstone
28	145.44	145.57	0.13	minor amount of anhydrite nodules		bedded vfgr sandstone	dolomite cemented vfgr sandstone	dolomite cemented vfgr sandstone
29	145.57	146.02	0.45	abundant nodules anhydrite	5	dolomite cemented vfgr sandstone	bedded vfgr sandstone	siltstone
30	146.40	146.63	0.23	nodular anhydrite at base becoming chicken wire upward	5	dolostone	siltstone	bedded vfgr sandstone
31	146.74	146.98	0.24	anhydrite nodules near top; prismatic gypsum overprint		vfgr sandstone	dolostone	dolostone
32	147.12	147.30	0.18	anhydrite nodules at top		laminated siltstone	dolostone	fgr sandstone
33	147.30	147.39	0.09	anhydrite nodules		fgr sandstone, bedded	laminated siltstone	dolostone
34	147.39	147.67	0.28	mosaic anhydrite with layers protonodules; gypsum overgrowth	5	dolostone	fgr sandstone, bedded	vfgr sandstone

35	148.00	148.04	0.04	anhydrite rock, overgrown with prismatic gypsum; growths inwards from base/top		anhydrite rock	sandstone sandstone	
36	148.04	148.35	0.31	anhydrite nodules and laminae		very fgr sandstone	anhydrite rock	dolostone
37	148.35	148.59	0.24	nodules anhydrite + prismatic gypsum	5	dolostone	very fgr sandstone	siltstone
38	148.64	148.69	0.05	nodules anhydrite	5	dolostone	siltstone	sandstone
39	148.69	149.20	0.51	nodules anhydrite; protonodules at base		very fgr sandstone	dolostone	dolostone
40	149.42	149.81	0.39	decreasing nodule % anhydrite/gypsum upwards; up to 80% at base		very fgr sandstone	dolostone	dolostone
41	149.81	149.90	0.09	anhydrite crystals in layers	5	dolostone	very fgr sandstone	very fgr sandstone
42	149.96	150.20	0.24	anhydrite rock at top, nodular downwards	5	dolostone	very fgr sandstone	very fgr sandstone
43	150.32	150.55	0.23	upwards decreasing % 50-20 anhydrite nodules	5	dolostone	very fgr sandstone	very fgr sandstone
44	150.55	151.08	0.53	beds anhydrite nodules at base; decreasing upwards %		very fgr sandstone	dolostone	dolostone
45	151.25	151.75	0.50	anhydrite nodules at base		very fgr sandstone	dolostone	anhydrite rock
46	151.75	152.42	0.67	40-50% anhydrite nodules, becoming anhydrite rock and chickenwire down; basal 12cm <1%	5	dolostone	very fgr sandstone	very fgr sandstone
47	152.42	152.56	0.14	anhydrite protonodules		laminated siltstone	dolostone	dolostone
48	152.56	152.95	0.39	anhydrite nodules, decrease upwards	5	dolostone	laminatede siltstone	anhydrite rock
49	152.95	152.96	0.01	anhydrite rock with prismatic gypsum	5	anhydrite rock	dolostone	dolostone
50	152.96	153.07	0.11	anhydrite nodules	5	dolostone	anhydrite rock	siltstone
51	153.07	153.09	0.02	anhydrite protonodules		siltstone	dolostone	dolostone
52	153.26	153.35	0.09	anhydrite protonodules in irregular layers		siltstone	dolostone	dolostone
53	153.35	153.48	0.13	small amounts anhydrite protonodules		very fgr sandstone	siltstone	dolostone
54	153.48	153.68	0.20	anhydrite nodules and protonodules in layers	5	dolostone	very fgr sandstone	sandstone
55	153.92	153.97	0.05	thin anhyrite layers		siltstone, laminated	dolostone	dolostone
56	153.97	154.16	0.19	anhydrite protonodules	5	dolostone, laminated	siltstone	siltstone
57	154.16	154.58	0.42	layers of aqnhydrite protonodules		siltstone, laminated	dolostone	siltstone
58	154.77	155.06	0.29	layers small anhydrite protonodules or cystals		wavy laminated siltstone	dolostone	sandstone
59	155.06	155.72	0.66	bands anhydrite nodulesjust beneath gradation of host to siltstone		sandstone to siltstone, fining up	sandstone	very fine gr sandstone
60	155.72	156.25	0.53	anhydrite nodules near base		sandstone	sandstone	dolostone
61	156.25	156.42	0.17	anhydrite nodules near base	5	dolostone	sandstone	sandstone
62	156.42	156.70	0.28	anhydrite nodules near base		coarsening up sandstone; very fine to fine	dolostone	dolostone
63	156.70	156.80	0.10	disturbed laminae and distributed crystals anhydrite	5	dolostone	sandstone	siltstone
64	156.80	157.45	0.65	anhydrite protonodules along lamination		siltstone, laminated	dolostone	dolostone
65	157.45	157.65	0.20	anhydrite protonodules at base	5	dolostone, laminated, with brecciated surfaces	siltstone	siltstone
66	157.96	158.12	0.16	chickenwire anhydrite	5	dolostone	siltstone	dolostone
67	158.12	158.29	0.17	anhydrite nodules		vfgr sandstone	dolostone	dolostone
68	158.29	158.55	0.26	small anhydrite crystals near base	5	dolostone, laminated	vfgr sandstone	siltstone
69	158.55	158.86	0.31	small gypsum nodule		siltstone, laminated	dolostone	dolostone
70	159.06	159.27	0.21	anhydrite crystals rich in centre, decreasing to top		siltstone, laminated	dolostone	dolostone
71	159.27	159.33	0.06	some anhydrite crystals	5	dolostone	siltstone	siltstone
72	159.33	159.50	0.17	anhydrite nodular decreasing up 40-1%		siltstone, laminated	dolostone	dolostone
73	159.50	159.62	0.12	nodular anhydrite	5	dolostone	siltstone	siltstone
74	159.62	159.88	0.26	nodules anhydrite		siltstone, laminated	dolostone	dolostone
75	160.16	160.53	0.37	small anhydrite crystals along lamination		siltstone, laminated	dolostone	dolostone

76	160.53	160.76	0.23	chickenwire and micronodular anhydrite; wavy laminated alternating beds; some very dark layers dolostone	5	dolostone	siltstone	vfgr sandstone
77	161.34	161.68	0.34	anhydrite crystals 1-2mm in patches along lamination; abundant in centre decreasing up and down		fine grained sandstone	dolostone	dolostone
78	162.25	162.59	0.34	thin layers anhydrite crystals near base	5	dolostone	siltstone	siltstone
79	162.79	162.85	0.06	layers of anhydrite crystals near base	4	fine grained sandstone	siltstone	dolostone
80	162.85	163.02	0.17	anhydrite in centre	5	dolostone, laminated	fine grained sandstone	siltstone
81	163.02	163.53	0.51	anhydrite crystals increasing upwards from 30-50%		siltstone, laminated, wavy lamination at top	dolostone	dolostone
82	163.53	163.63	0.10	layers of anhydrite crystals	5	dolostone	siltstone	siltstone
83	163.63	163.76	0.13	small nodules along lamination		siltstone	dolostone	dolostone
84	163.97	164.28	0.31	layered anhydrite, soft sediment deformed	4	siltstone interbeds	dolostone	vfgr sandstone
85	165.18	166.22	1.04	scattered anhydrite nodules		very fine grained sandstone	dolostone	dolostone
86	166.22	166.49	0.27	thin layer small compressed nodules anhydrite near top	5	dolostone	very fgr sandstone	fgr sandstone
87	166.49	166.74	0.25	Common dispersed anhydrite crystals up to 4mm	4	fine grained sandstone, laminated	dolostone	dolostone
88	166.74	166.95	0.21	nodules anhydrite in centre, deformed laminae of anhydrite in upper part	5	dolostone	fine grained sandstone	siltstone
89	167.64	167.85	0.21	anhydrite crystals and laminae decreasing upwards 25-1%	4	very fine grained sandstone	fine grained sandstone	dolostone
90	167.85	168.08	0.23	anhydrite rock, increasing % upward	5	small amount dolostone at base and top	vfgr sandstone	siltstone
91	168.32	168.43	0.11	chickenwire anhydrite at top, nodular in lower part	5	dolostone	vfgr sandstone	dolostone
92	168.43	168.56	0.13	anhydrite crystals	5	dolostone	dolostone	fgr sandstone
93	168.93	169.08	0.15	laminae anhydrite crystals	4	laminae siltstone and dolostone	siltstone	dolostone
94	169.08	169.18	0.10	anhydrite crystals; %decrease upward	4	laminated anhydrite and siltstone	laminated siltstone and anhydrite	siltstone
95	169.18	169.20	0.02	anhydrite aggregates, small		striped siltstone	laminated anhydrite and siltstone	dolostone
96	169.27	169.33	0.06	nodules anhydrite near base		fgr sandstone, bedded	dolostone	dolostone
97	169.33	169.45	0.12	anhydrite nodules concentrated at base	5	dolostone	sandstone	vfgr sandstone
98	169.45	169.95	0.50	nodules anhydrite top and in lower part		vfgr sandstone	dolostone	dolostone
99	169.95	170.07	0.12	anhydrite nodules	5	dolostone	sandstone	sandstone
100	170.20	170.45	0.25	sparse anhydrite nodules in centre		sandstone, slightly coarsening upward	sandstone	dolostone
101	170.80	171.01	0.21	anhydrite nodules		vfgr sandstone, wavy laminated	sandstone	sandstone
102	171.01	171.21	0.20	layered anhydrite rock	4	sandy siltstone	sandstone	dolostone
103	171.21	171.65	0.44	anhydrite crystals in top 10cm	5	dolostone	sandstone	siltstone
104	173.47	173.73	0.26	in lower part nodular anhydrite 50%; almost none at top	5	dolostone	siltstone, laminated	siltstone laminated
105	174.13	174.38	0.25	small % anhydrite nodules	5	dolostone, massive	siltstone	siltstone
106	174.49	174.72	0.23	some small protonodules anhydrite	5	dolostone, massive	siltstone	vfgr sandstone
107	174.84	174.97	0.13	some small protonodules anhydrite	5	dolostone, massive	sandstone	vfgr sandstone
108	176.74	177.02	0.28	nodules anhydrite	5	dolostone	dolostone	siltstone
109	177.20	178.20	1.00	nodules and mosaic anhydrite; varying % in beds	5	dolostone	siltstone	siltstone
110	178.23	178.74	0.51	nodules anhydrite	5	dolostone	siltstone	siltstone

111	178.80	179.04	0.24	chickenwire anhydrite, becoming nodular to base	5	dolostone	siltstone	dolostone
112	179.04	179.32	0.28	nodular anhydrite, % decrease up to 30 from c90; but increase in nodule size	5	dolostone	dolostone	siltstone
113	179.32	179.40	0.08	anhydrite nodule		siltstone, laminated	dolostone	dolostone
114	179.40	179.90	0.50	chickenwire and mosaic anhydrite	5	dolostone	siltstone	siltstone
115	180.07	180.18	0.11	c 7% anhydrite nodules	5	dolostone	siltstone	dolostone
116	180.18	180.51	0.33	chickenwire to mosaic anhydrite	5	dolostone	dolostone	dolostone
117	180.51	180.73	0.22	mosiac anhydrite, up to 80%	5	dolostone	dolostone	siltstone
118	180.77	181.60	0.83	small nodules anhydrite	5	dolostone, in part laminated	siltstone	vfgr sandstone
119	182.37	183.67	1.30	nodules and mosaic anhydrite		sandstone, silty	dolostone	sandstone
120	183.67	184.51	0.84	nodules anhydrite		sandstone, fgr	sandstone	sandstone
121	184.86	185.09	0.23	anhydrite, massive	5	dolostone	sandstone	sandstone
122	185.20	185.45	0.25	anhydrite massive	?5	?dolostone	sandstone	sandstone
123	187.64	187.79	0.15	anhydrite, massive	?5	?dolostone	siltstone	dolostone
124	187.89	188.80	0.91	anhydrite nodules	5	dolostone	dolostone	siltstone
125	189.05	189.80	0.75	massive anhydrite	5	dolostone	siltstone	sandstone
126	190.07	190.83	0.76	anhydrite patches (?nodules)		sandstone, fine-grained	dolostone	dolostone
127	196.76	198.45	1.69	anhydrite patches (?nodules)		sandstone, fine-grained	dolostone	dolostone
128	198.57	199.36	0.79	an hydrite breccia (?mosaic)		sandstone, fgr & siltstone	dolostone	dolostone

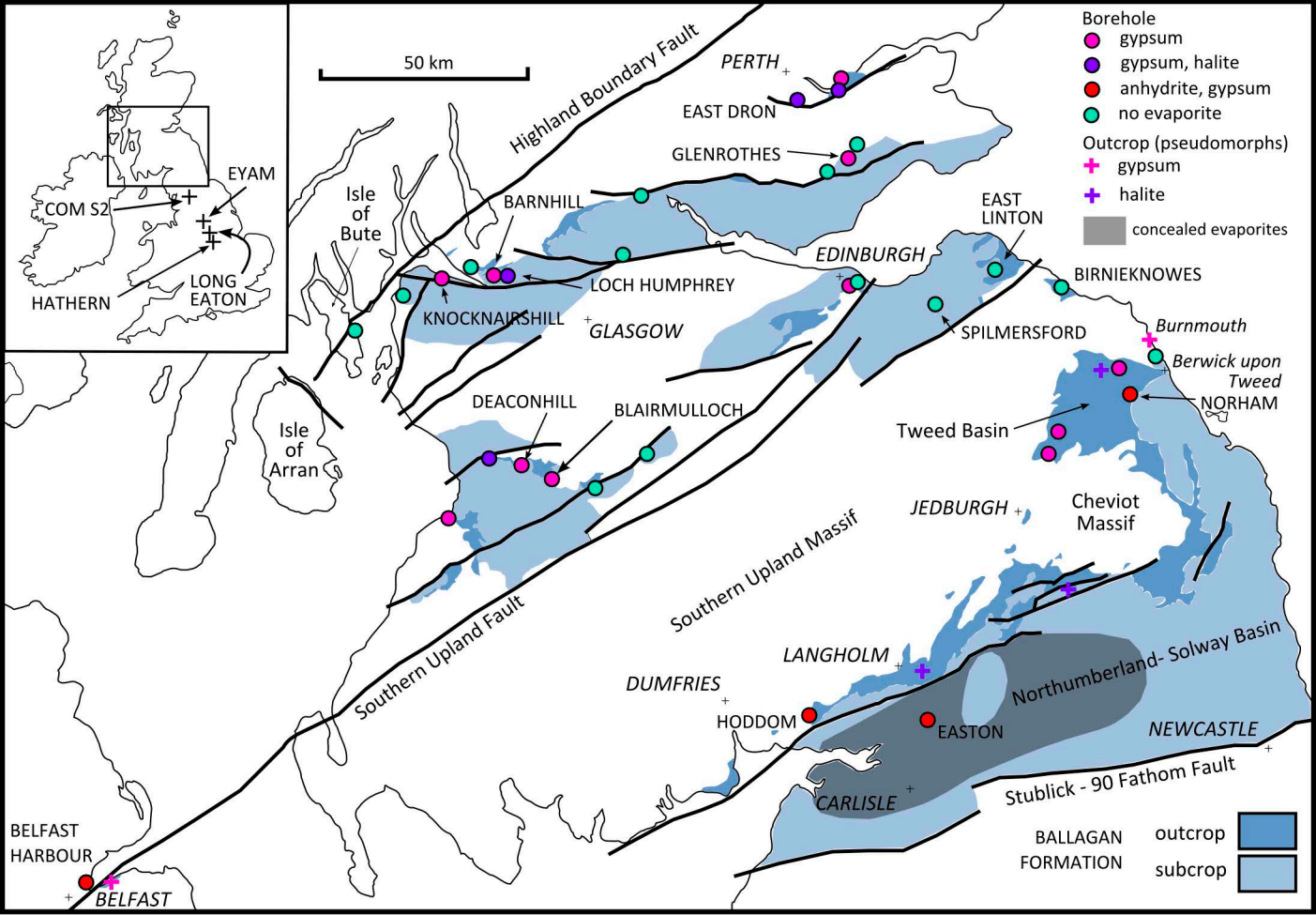
Borehole
gypsum
gypsum, halite
anhydrite, gypsum
no evaporite
Outcrop (pseudomorphs)
gypsum
halite
concealed evaporites
50 km
Highland Boundary Fault
PERTH
EAST DRON
GLENROTHES
BARNHILL
Isle of Bute
LOCH HUMPHREY
KNOCKNAIRSHILL
GLASGOW
EDINBURGH
EAST LINTON
BIRNIEKNOWES
SPILMERSFORD
Burnmouth
Berwick upon Tweed
NORHAM
Tweed Basin
DEACONHILL
BLAIRMULLOCH
Isle of Arran
JEDBURGH
Cheviot Massif
Southern Upland Massif
Southern Upland Fault
LANGHOLM
DUMFRIES
HODDOM
EASTON
Northumberland- Solway Basin
NEWCASTLE
Stublick - 90 Fathom Fault
CARLISLE
BELFAST HARBOUR
BELFAST
BALLAGAN FORMATION
outcrop
subcrop
EYAM
COM S2
HATHERN
LONG EATON

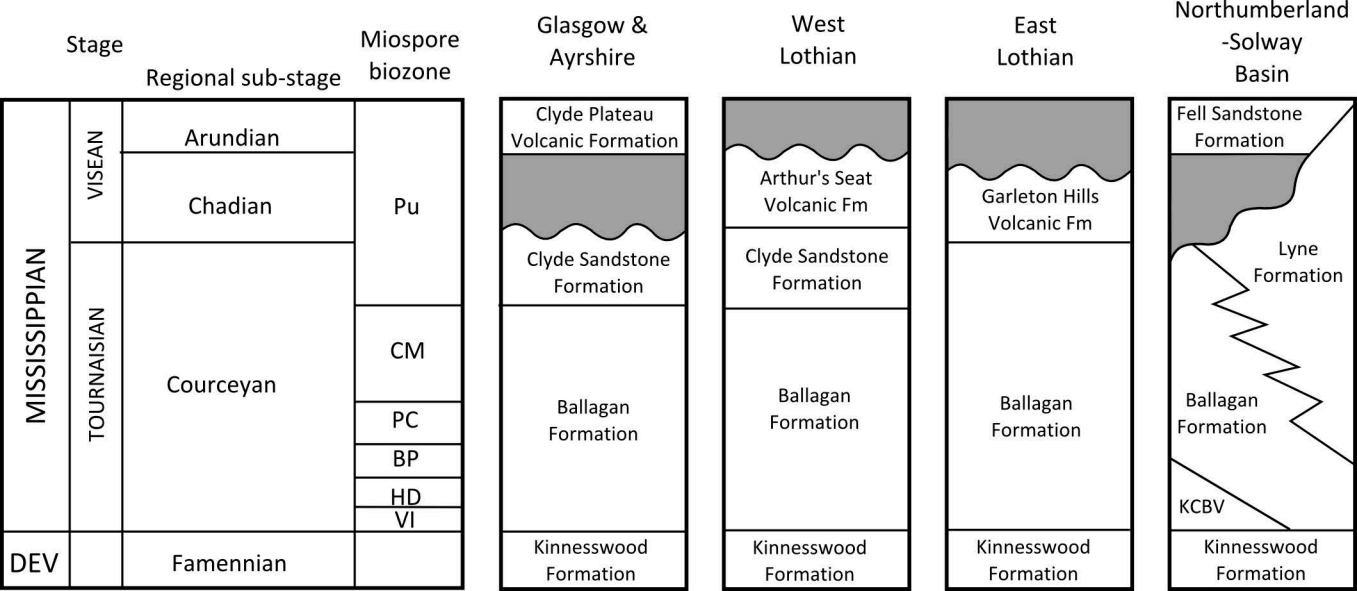
Stage
Regional sub-stage
Miospore biozone
Glasgow & Ayrshire
West Lothian
East Lothian
Northumberland -Solway Basin
MISSISSIPPIAN
DEV
VISEAN
TOURNAISIAN
Arundian
Chadian
Courceyan
Famennian
Pu
CM
PC
BP
HD
VI
Clyde Plateau Volcanic Formation
Clyde Sandstone Formation
Ballagan Formation
Kinnesswood Formation
Arthur's Seat Volcanic Fm
Clyde Sandstone Formation
Ballagan Formation
Kinnesswood Formation
Garleton Hills Volcanic Fm
Ballagan Formation
Kinnesswood Formation
Fell Sandstone Formation
Lyne Formation
Ballagan Formation
KCBV
Kinnesswood Formation

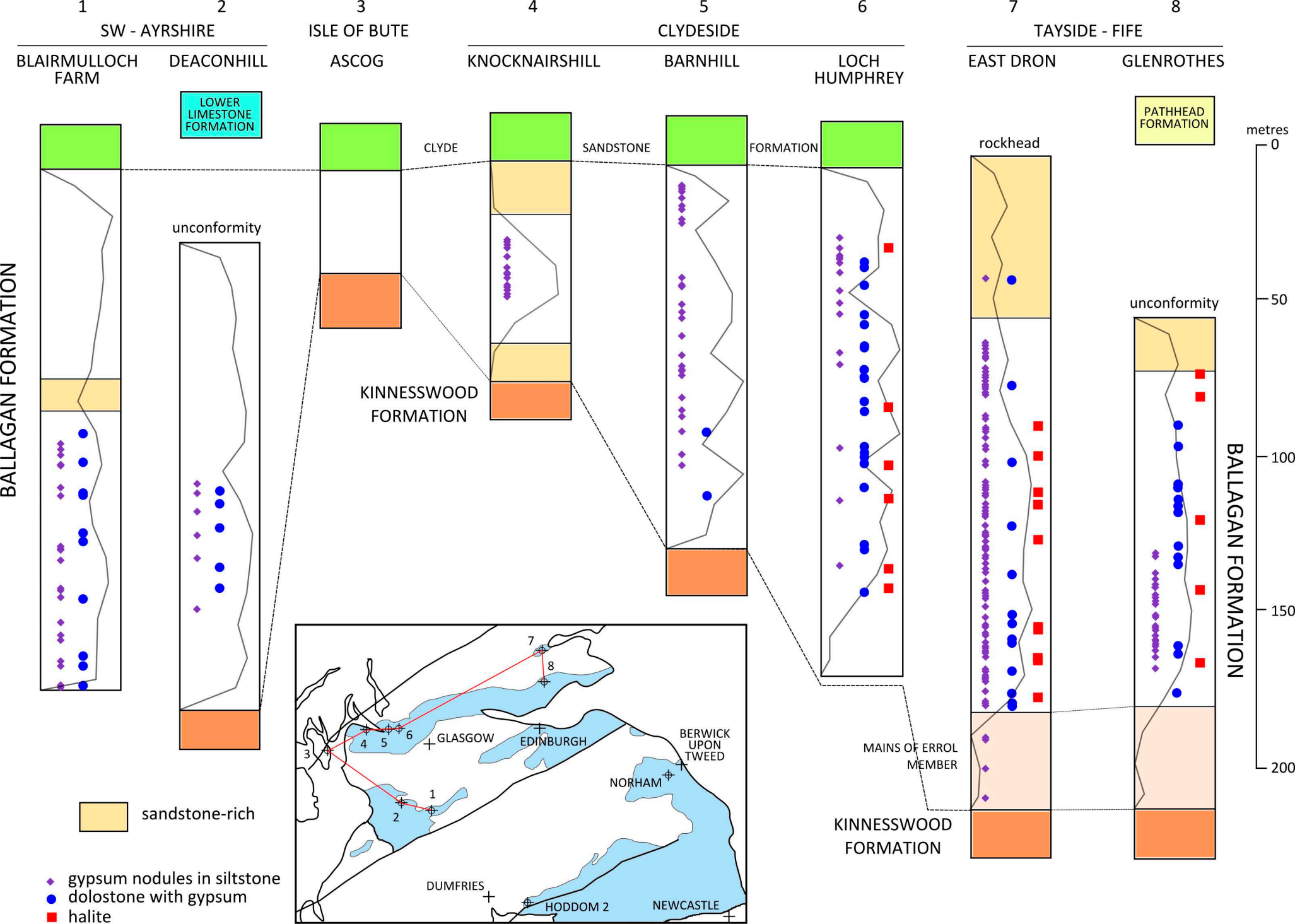
1
2
3
4
5
6
7
8
SW - AYRSHIRE
ISLE OF BUTE
CLYDESIDE
TAYSIDE - FIFE
BLAIRMULLOCH FARM
DEACONHILL
ASCOG
KNOCKNAIRSHILL
BARNHILL
LOCH HUMPHREY
EAST DRON
GLENROTHES
LOWER LIMESTONE FORMATION
PATHHEAD FORMATION
metres
0
50
100
150
200
BALLAGAN FORMATION
unconformity
CLYDE
SANDSTONE
FORMATION
KINNESSWOOD FORMATION
rockhead
unconformity
BALLAGAN FORMATION
MAINS OF ERROL MEMBER
KINNESSWOOD FORMATION
GLASGOW
EDINBURGH
BERWICK UPON TWEED
NORHAM
DUMFRIES
HODDOM 2
NEWCASTLE
sandstone-rich
gypsum nodules in siltstone
dolostone with gypsum
halite

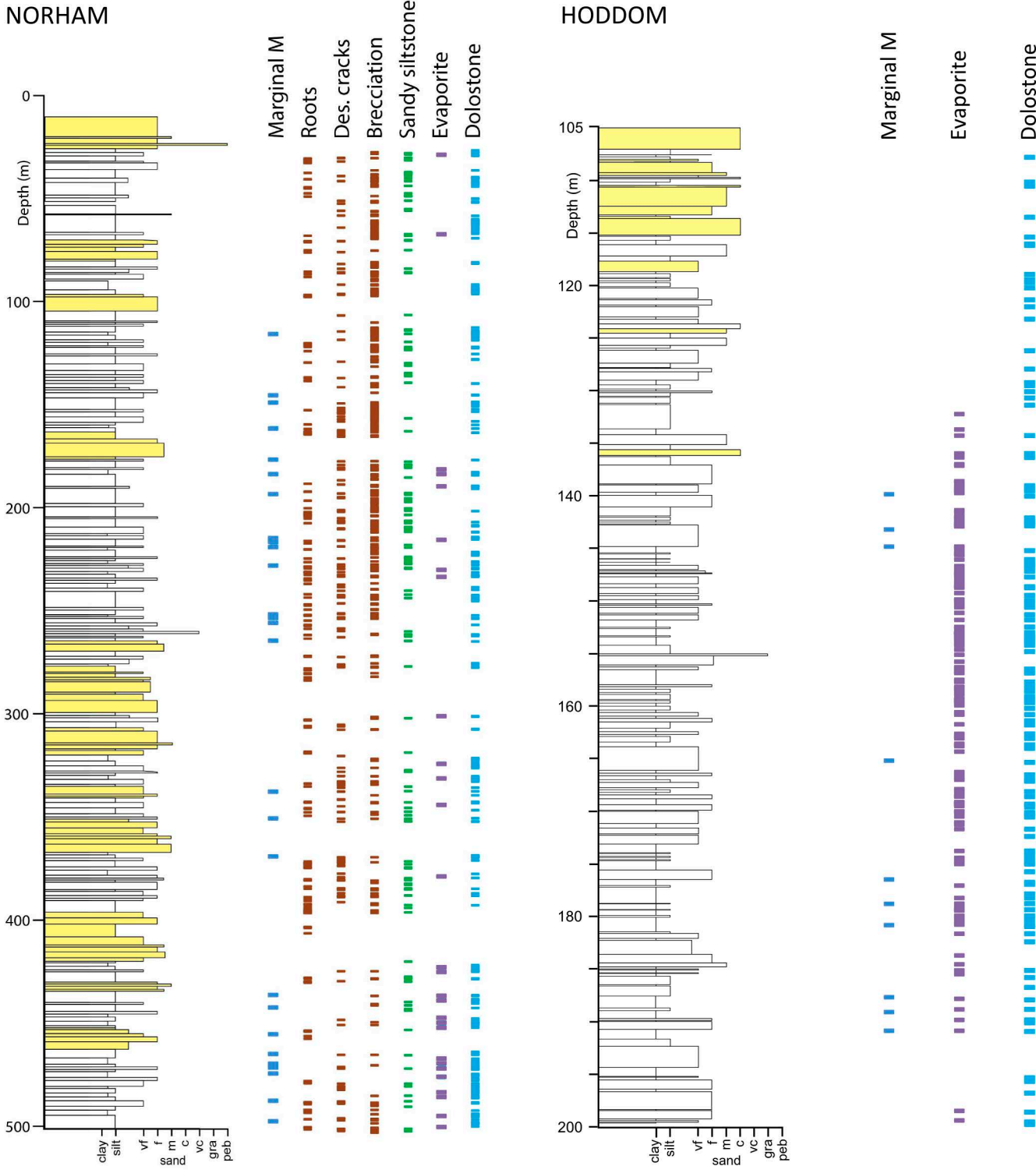
NORHAM
Depth (m)
0
100
200
300
400
500
clay
silt
vf
f
m
c
vc
gra
peb
sand
Marginal M
Roots
Des. cracks
Brecciation
Sandy siltstone
Evaporite
Dolostone
HODDOM
Depth (m)
105
120
140
160
180
200
clay
silt
vf
f
m
c
vc
gra
peb
sand
Marginal M
Evaporite
Dolostone

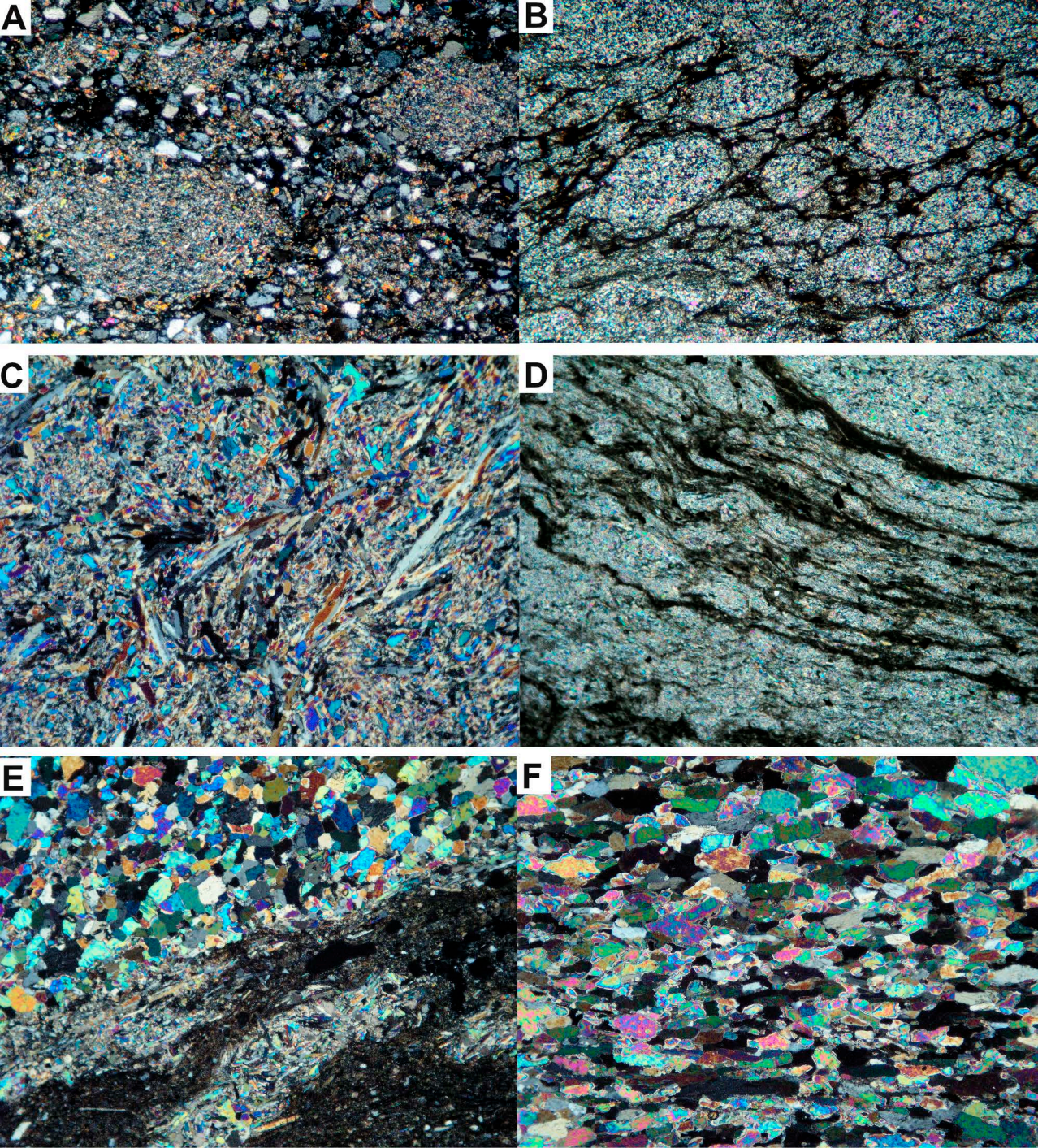
A
B
C
D
E
F

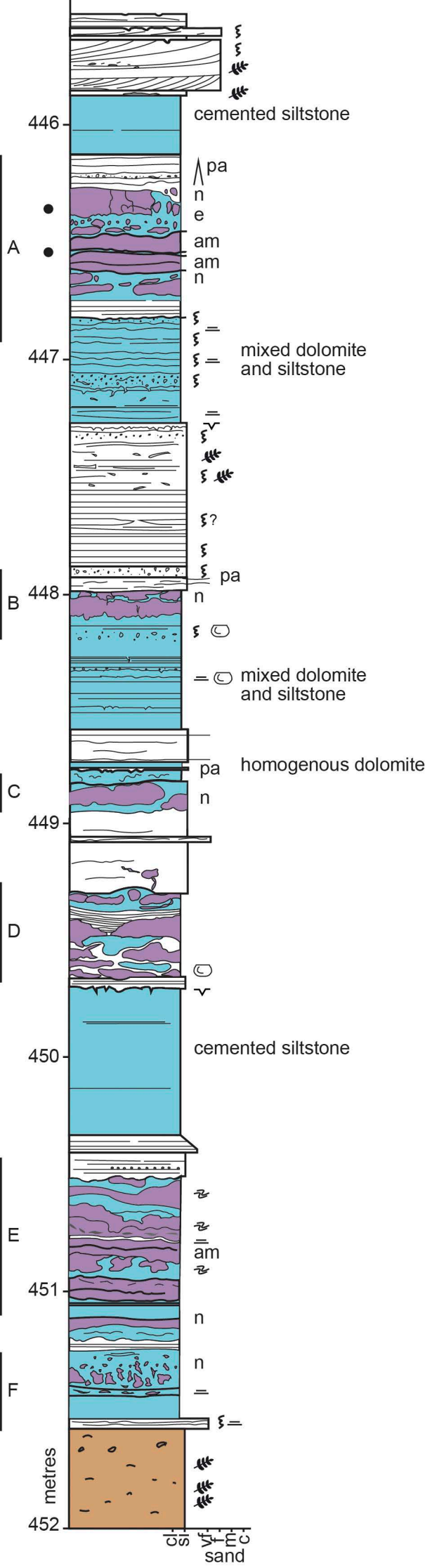
446
447
448
449
450
451
452
A
B
C
D
E
F
cemented siltstone
pa
n
e
am
am
n
mixed dolomite
and siltstone
pa
n
mixed dolomite
and siltstone
pa
homogenous dolomite
n
cemented siltstone
am
n
n
metres
cl
si
vf
f
m
c
sand

evaporite beds, gypsum or anhydrite

dolostones

sandy siltstones

parallel laminated bedding

convoluted bedding

brecciation

plant fragments

bioturbation

ostracods

am microbial mat

n nodule

pa anhydrite protonodules

A

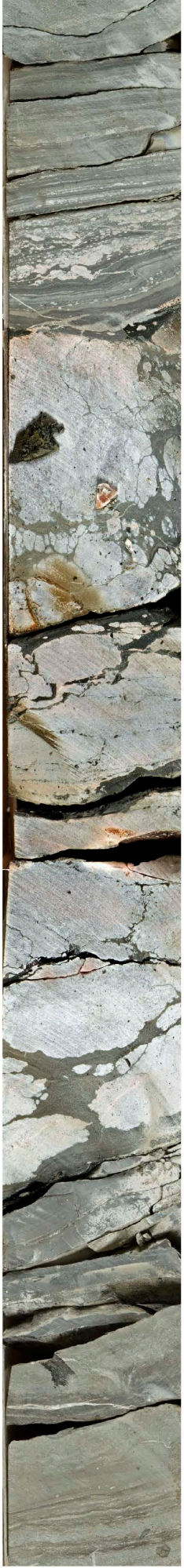

B

C

D

E

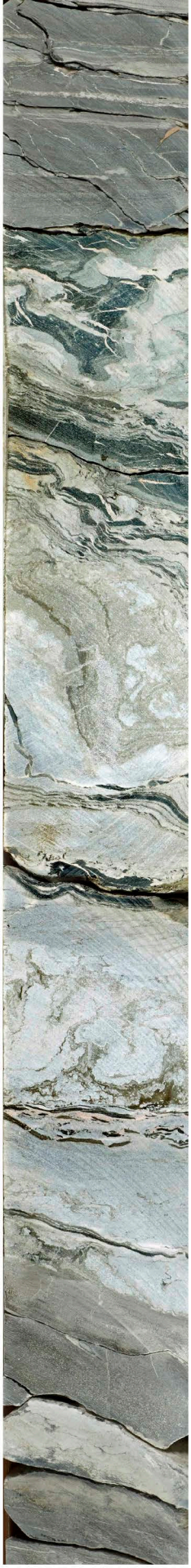

F


A


C


D

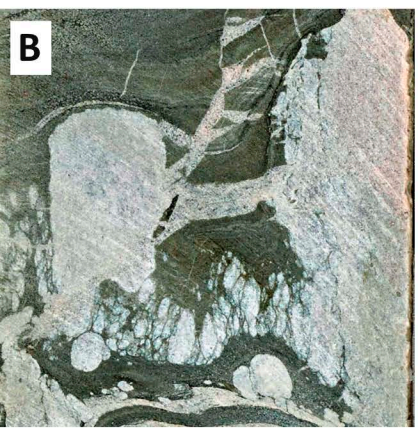
B


F


E


G

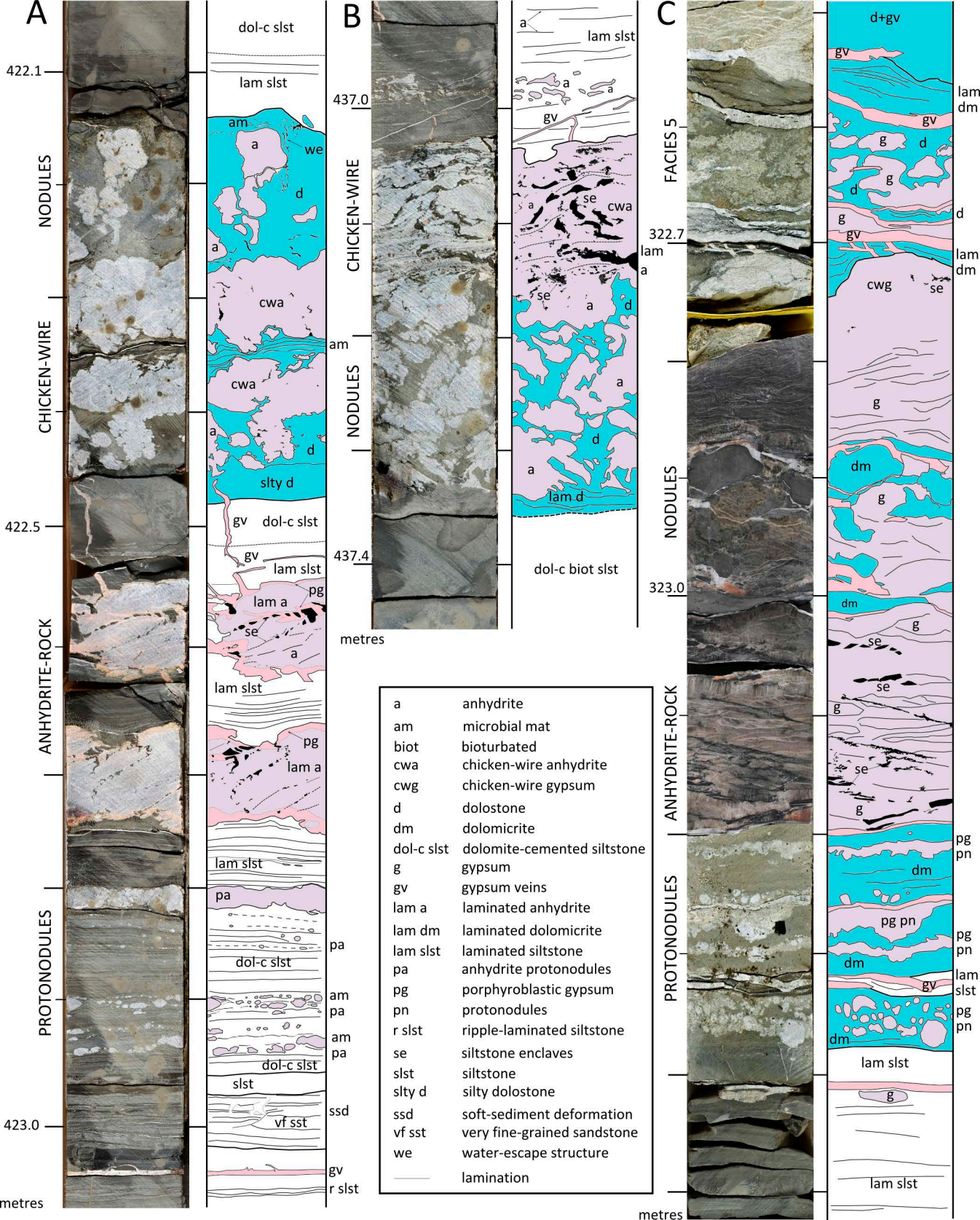

a	anhydrite
am	microbial mat
biot	bioturbated
cwa	chicken-wire anhydrite
cwg	chicken-wire gypsum
d	dolostone
dm	dolomicrite
dol-c slst	dolomite-cemented siltstone
g	gypsum
gv	gypsum veins
lam a	laminated anhydrite
lam dm	laminated dolomicrite
lam slst	laminated siltstone
pa	anhydrite protonodules
pg	porphyroblastic gypsum
pn	protonodules
r slst	ripple-laminated siltstone
se	siltstone enclaves
slst	siltstone
slty d	silty dolostone
ssd	soft-sediment deformation
vf sst	very fine-grained sandstone
we	water-escape structure
	lamination

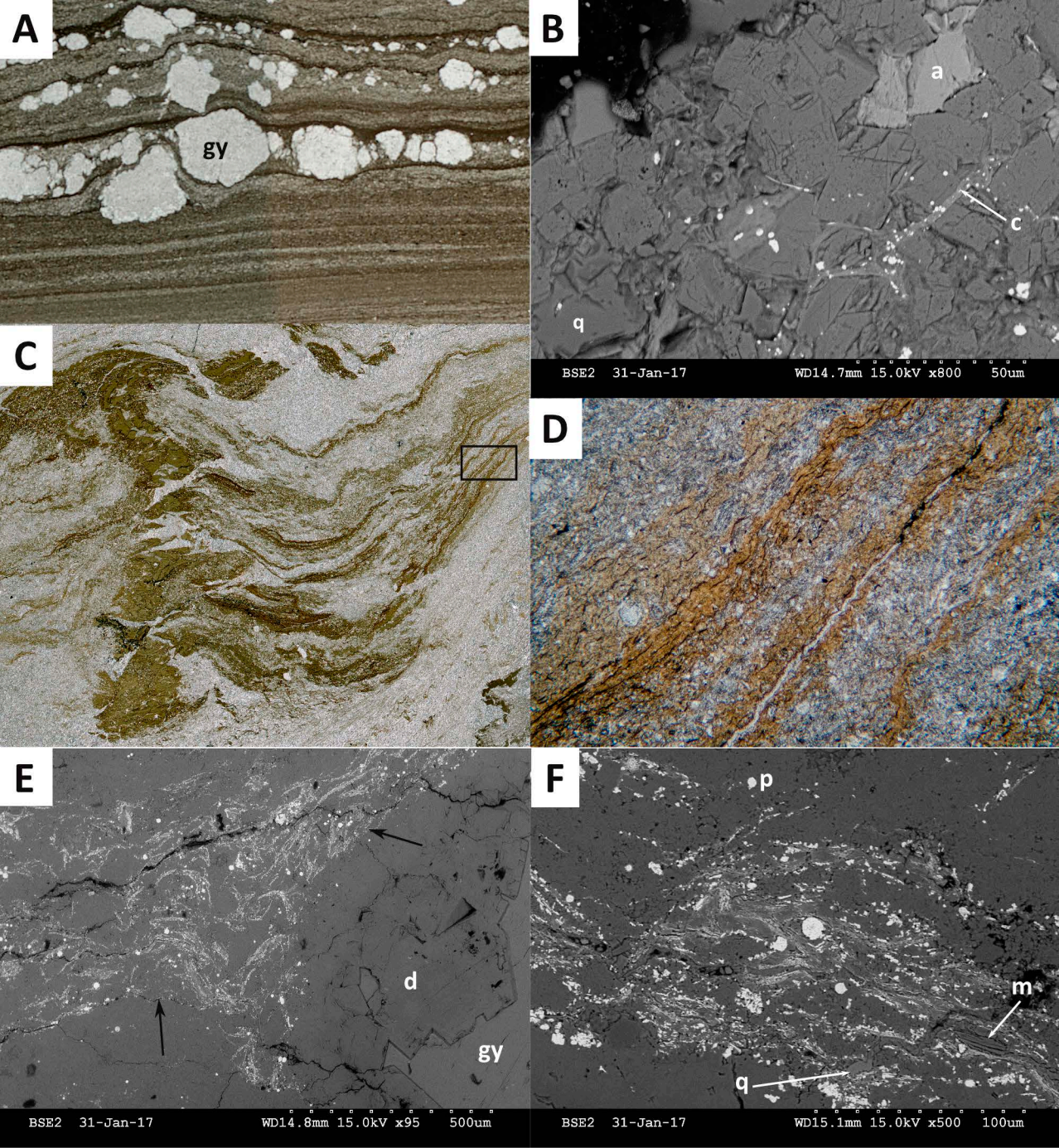
A
gy
B
a
c
q
BSE2 31-Jan-17 WD14.7mm 15.0kV x800 50um
C
D
E
d
gy
BSE2 31-Jan-17 WD14.8mm 15.0kV x95 500um
F
p
m
q
BSE2 31-Jan-17 WD15.1mm 15.0kV x500 100um

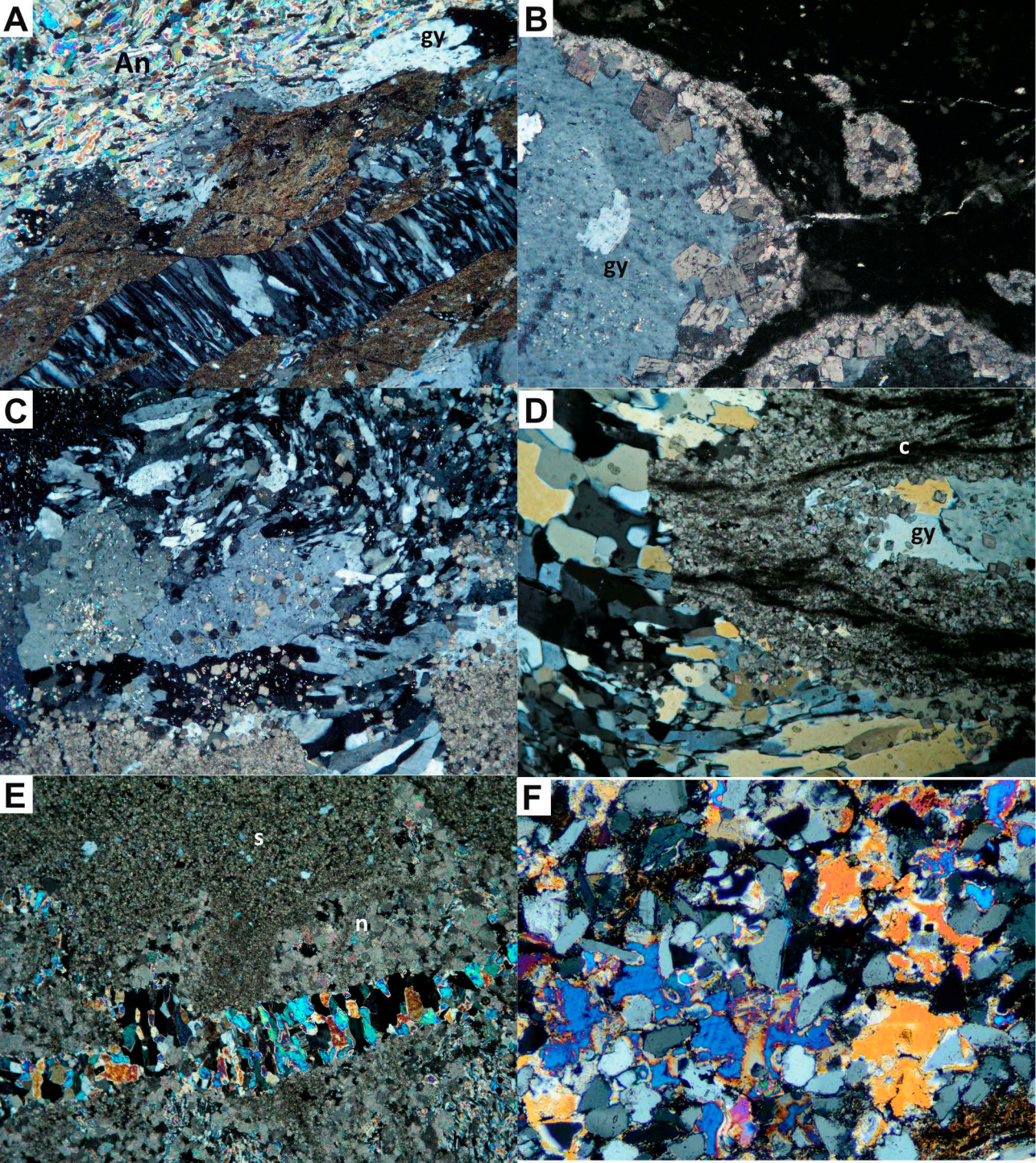
A
An
gy
B
gy
C
D
c
gy
E
s
n
F